Non-Heme High-Spin {FeNO}$^{6-8}$ Complexes: One Ligand Platform Can Do It All

Amy L. Speelman,[a$] Corey J. White,[a$] Bo Zhang,[b] E. Ercan Alp,[c] Jiyong Zhao,[c] Michael Hu,[c] Carsten Krebs,[b] James Penner-Hahn,[a] and Nicolai Lehnert [a*]

[a] Department of Chemistry and Department of Biophysics, University of Michigan, Ann Arbor, MI 48109-1055. Email: lehnertn@umich.edu.
[b] Department of Chemistry and Department of Biochemistry and Molecular Biology, The Pennsylvania State University, University Park, Pennsylvania, 16802.
[c] Advanced Photon Source, Argonne National Laboratory, Argonne, Illinois, 60439.

Supporting Information

Table of Contents

Synthetic, Physical, and DFT Procedures

TMG$_3$tren hs-{FeNO}$^{6-8}$ (**1-3**) S5-S6

[Fe(TMG$_2$dien)(OTf)](OTf) (**4**) S6

H{FeNO}^{8} (**5**) and Me{FeNO}^{8} (**6**) S7

Physical Measurements S7-S13

DFT Calculations S15-S16

EXAFS Measurements

EXAFS-FT of {FeNO}^{7} and {FeNO}^{6} ligand simulations (Figure S1) S12

EXAFS-k^3 fits of hs-{FeNO}^{6}, hs-{FeNO}^{7}, hs-{FeNO}^{8}, and H{FeNO}^{8} (Figure S2) S14

EXAFS-FT of hs-{FeNO}^{6}, hs-{FeNO}^{7}, hs-{FeNO}^{8}, and H{FeNO}^{8} (Figure S3) S15

SI Figures and Tables for *Section 2.1*

EPR of **1**, **3**, and the decomposition product of **3** (Figure S4) S17

Solution IR of the decomposition product of **3** (Figure S5) S17

DFT calculated geometric and spectroscopic parameters for **1-3** (Table S1) S18

SI Figures and Tables for *Section 2.2*

FTIR of **4** and of the ferrous precursor (Figure S6) S19

UV-Vis of **4** (Figure S7) S19

X-band EPR of **4** (Figure S8) S20

^{1}H-NMR of **4** in CD_2Cl_2 (Figure S9) S21

Solution IR of the decomposition product of **2** (Figure S10) S22

^{1}H-NMR following the decomposition of **2** in CD_3CN (Figure S11) S23

Crystallographic data and refinement factors for **4** (Table S2) S24

SI Figures and Tables for *Section 2.3*

DFT-calculated *D*, *E/D*, and hyperfine coupling constants (*A*) for **1-3** (Table S3) S25

Euler angles for rotation of the EFG/HFC tensors of **1-3** to their ZFS tensors (Table S4) S26

Variable field Mössbauer of **3** showing impurity fits (Figure S12) S27

Variable field Mössbauer of **3** (Figure S13) S28

Comparison of DFT and experimental Mössbauer parameters for **3** (Table S5) S28

SI Figures and Tables for *Section 2.5*

IR spectra of **1** under different conditions (Figure S14) S29

Experimental and DFT predicted NRVS of $\{^{57}FeNO\}^{7}$ and $\{^{57}Fe^{15}N^{18}O\}^{7}$ (Figure S15)..... S30
Experimental and DFT predicted NRVS of $\{^{57}FeNO\}^{8}$ and $\{^{57}Fe^{15}N^{18}O\}^{8}$ (Figure S16)..... S30
Solution IR and KBr spectra of $\{^{57}FeNO\}^{8}$ and $\{^{57}Fe^{15}N^{18}O\}^{8}$ (Figure S17)..... S31
Experimental and DFT predicted NRVS of $\{^{57}FeNO\}^{6}$ and $\{^{57}Fe^{15}N^{18}O\}^{6}$ (Figure S18)..... S32
SI Figures and Tables for *Section 2.6*
UV-Vis bulk electrolysis showing the conversion of **1** to **2** (Figure S19)..... S33
UV-Vis spectro-electrochemistry showing the conversion of **1** to **3** (Figure S20)..... S33
Magnetic saturation curves for band 2 (651 nm) of **1** (Figure S21) S34
Magnetic saturation curves for band 1 (856 nm) of **1** (Figure S22) S34
Correlated Gaussian deconvolution of the UV-Vis and MCD spectra of **2** (Figure S23) S35
Parameters for the correlated fit of the UV-Vis and MCD spectra of **2** (Table S6) S35
VTVH saturation curves for **2** (Figure S24) S36
Comparison of UV-Vis and MCD spectra of **1** (Figure S25) S37
Comparison of UV-Vis and MCD spectra of **2** (Figure S26) S37
Correlated Gaussian deconvolution of the UV-Vis and MCD spectra of **3** (Figure S27) S38
Parameters for the correlated fit of the UV-Vis and MCD spectra of **3** (Table S7) S38
Variable temperature MCD spectra of **3** (Figure S28)..... S39
SI Figures and Tables for *Section 2.7*
Solution IR for the reaction of **1** with $[HNEt_3][PF_6]$ and $[OMe_3][BF_4]$ (Figure S29) S40
UV-Vis showing the reversible protonation of **2** to **5** (Figure S30) S41
UV-Vis showing the stability of **5** at -70 ^{o}C (Figure S31)..... S41
UV-Vis of the decomposition of **5** at RT in the presence of $HNEt_3PF_6$ (Figure S32)..... S42
UV-Vis titration of **2** with $[OMe_3][BF_4]$ to **6** (Figure S33) S43
UV-Vis showing the stability of **6** at -45 ^{o}C (Figure S34)..... S43
Weak-field Mössbauer of **6** (Figure S35) S44
EPR following the reduction of **1** to **2** and protonation of **2** to **5** (Figure S36) S45
Correlated Gaussian deconvolution of the UV-Vis and MCD spectra of **5** (Figure S37) S46
Parameters for the correlated fit of the UV-Vis and MCD spectra of **5** (Table S8) S46
VTVH saturation curves for **5** (Figure S38) S47
Comparison of the MCD spectra of **1, 5,** and **6** (Figure S39)..... S48
Comparison of the MCD spectra of **1, 2,** and **5** (Figure S40)..... S49

Solution IR spectra of the decomposition product of **5** at RT (Figure S41) S50-S51
DFT predicted structural parameters of different protonated versions of **5** (Table S9)..... S52
DFT predicted structural parameters of different methylated versions of **5** (Table S10)..... S52
Experimental and DFT-calculated Mössbauer data for TMG_3tren complexes (Table S11)... S52
Correlation of experimental and DFT-calculated isomer shifts for **6** (Figure S42)..... S53
DFT-optimized coordinates of:
S=2 $[Fe(TMG_3tren)(O)]^{2+}$ (Table S12) S54-S55
S=2 $\{FeHNO\}^8$ (Table S13) S56-S57
S=1 $\{FeHNO\}^8$ (Table S14) S58-S59
S=2 $\{FeNOH\}^8$ (Table S15) S60-S61
S=1 $\{FeNOH\}^8$ (Table S16) S62-S63
S=2 $\{FeCH_3NO\}^8$ (Table S17) S64-S65
S=1 $\{FeCH_3NO\}^8$ (Table S18) S66-S67
S=2 $\{FeNOCH_3\}^8$ (Table S19) S68-S69
S=1 $\{FeNOCH_3\}^8$ (Table S20) S70-S71
4-coordinate S=1 $H\{FeNO\}^8$ (Table S21) S72-S73
5-coordinate S=1 $H\{FeNO\}^8$ (Table S22) S74-S76
S=1 $[Fe(TMG_3tren)(CN)]^{3+}$ (Table S23) S77-S78
S=2 $[Fe(TMG_3tren)(CH_3CN)]^{2+}$ (Table S24) S79-S80

Experimental Details

General Synthetic Procedures

In general, reactions were performed under dinitrogen or argon using inert gas (Schlenk) techniques or under a dinitrogen atmosphere in an MBraun glovebox equipped with a circulating purifier (O_2, H_2O < 10 ppm). Solvents and reagents were purchased and used as supplied except as follows. Acetonitrile, propionitrile, butyronitrile, dichloromethane, and hexanes were distilled from calcium hydride, and diethyl ether was distilled from sodium benzophenone. All solvents were freeze-pump-thawed to remove dioxygen, and stored over 3 Å (CH_3CN, EtCN, PrCN) or 4 Å (Et_2O, CH_2Cl_2, hexanes) molecular sieves in a glovebox. Anhydrous acetone (99.8%, extra dry) was purchased from Acros, cannula transferred to a dry Schlenk flask, and freeze-pump-thawed to remove dioxygen. Nitric oxide (Cryogenic Gases Inc., 99.5%) was purified by passage through an ascarite II column (NaOH on silica) and then through a cold trap at −80 °C in order to remove higher nitrogen oxide impurities. Nitric oxide-^{15}NO (Cambridge Isotope Labs) and -$^{15}N^{18}O$ (Sigma-Aldrich) were used without further purification. Metallocene reductants ($CoCp_2$, $CoCp^*_2$, and $CrCp^*_2$) were purified by vacuum sublimation at approximately 50 °C and stored in the dark under inert atmosphere at −35 °C prior to use. $[HNEt_3][PF_6]$ was synthesized following a literature procedure.[1]

Synthesis of TMG_3tren hs-{FeNO}$^{6-8}$ Complexes

The syntheses of the TMG_3tren hs-{FeNO}$^{6-8}$ complexes followed previously published procedures.[2,3] Solid samples of the hs-{FeNO}^{8} complex **2** were generated by the addition of a slight excess of $CrCp^*_2$ to the hs-{FeNO}^{7} complex **1**, typically in the 5-20 mM concentration range in CH_3CN or CH_2Cl_2, pre-chilled to −35 °C in a freezer. The solvent was then removed under vacuum, and the resulting brown powder was washed into a fritted glass funnel with diethyl

ether. This crude material was used without further purification for NRVS and EXAFS measurements. Solution Mössbauer samples (5 mM in ^{57}Fe in 1:1 propionitrile:butyronitrile) were generated as previously described.[3] MCD samples of the hs-{FeNO}^{7} complex **1** were generated by dissolving the complex in 1:1 propionitrile:butyronitrile; data were collected at two different concentrations (5mM and 1mM) in order to capture the magnetic saturation behavor of both high- and low-intensity features. The MCD sample of the hs-{FeNO}^{8} complex (**2**) was prepared by performing bulk electrolysis on 2 mM **1** in 1:1 propionitrile:butytonitrile containing 0.1 M NBu_4ClO_4 as supporting electrolyte. The MCD sample of the hs-{FeNO}^{6} complex **3** was prepared by oxidation of 2 mM **1** with 1.3 equivalents of thianthreyl tetrafluoroborate.

Synthesis of [Fe(TMG$_2$dien](NO)(OTf)](OTf) (4)

[Fe(TMG$_2$dien)(OTf)$_2$] was generated by metallation of TMG$_2$dien with $FeCl_2$, followed by metathesis with thallium trifluoromethanesulfonate following literature procedures.[4]

Under an inert atmosphere, 200 mg (0.30 mmol) of [Fe(TMG$_2$dien)(OTf)$_2$] was dissolved in a minimal volume of CH_2Cl_2 and filtered to remove insoluble impurities. The solution was then exposed to excess NO gas, causing it to change color from light brown to dark green. The reaction was stirred for 45 minutes, at which point 36 mL of hexanes was syringed into the flask, causing the product to precipitate. The reaction was stored at –35 °C overnight and then filtered, affording 139 mg (66.7% yield) of the title compound as green needles. Single crystals suitable for X-ray diffraction were grown by layering a concentrated CH_2Cl_2 solution of **4** with hexanes at room temperature. ^{1}H NMR (400 MHz, CD_2Cl_2, all peaks appear as broad singlets): δ = 202, 187, 153, 131, 125, 92, 72, 39, 38, 36, 18, 14 ppm (see Figure S9); FT-IR (KBr pellet): ν(N-O) = 1770 cm^{-1} (see Figure S6); Elemental analysis: Expected for $C_{17}H_{35}F_6FeN_8O_7S_2$ • 0.5 CH_2Cl_2 : C, 28.50; H, 4.92; N, 15.20; Found: C, 28.11; H, 5.05; N, 14.91.

Generation of the H{FeNO}^{8} and Me{FeNO}^{8} Complexes

Except where noted, all manipulations of the H{FeNO}^{8} and Me{FeNO}^{8} complexes were performed in a glovebox in a dry ice / hexanes bath (–70 °C) or a dry ice / silicone oil bath (–40 °C). A solution Mössbauer sample of H{FeNO}^{8} (**5**) was generated via the room temperature reduction of 4.0 mM **1** in 1:1 propionitrile:butyronitrile with 1.5 equivalents of $CoCp^*$. The resulting hs-{FeNO}^{8} stock solution was cooled to -80 ºC and 2.0 equivalents of $HNEt_3PF_6$ were added to the solution, giving **5**. A Mössbauer sample of the Me{FeNO}^{8} complex **6** was generated by the addition of 3.7 equivalents of OMe_3BF_4 to the remaining 4mM {FeNO}^{8} solution at -80 ºC. EXAFS samples of H{FeNO}^{8} were generated similarly, via reduction of 4.0 mM **1** in acetone with 1.0 equivalent of $CoCp^*_2$ to generate **2**, followed by the addition of 1.0 equivalent of $HNEt_3PF_6$ at -80 ºC. The MCD sample of H{FeNO}^{8} was generated via reduction of 2 mM **1** at -80 ºC with 1.2 equivalents of $CoCp^*_2$ followed by addition of 1.6 equivalents of $HNEt_3PF_6$. The CH_3{FeNO}^{8} MCD sample was generated in a similar manner, using OMe_3BF_4 as the methyl source.

Physical Measurements

Infrared spectra of solid samples were obtained from KBr disks on Perkin-Elmer BX, GX, or RX1 spectrometers, and the IR spectra of solution samples were obtained in cells equipped with CaF_2 windows on the same instruments. Proton NMR spectra were recorded on a Varian MR 400 MHz instrument or a Varian VNMRS 500 MHz instrument. UV-Visible spectra were recorded using an Analytical Jena Specord S600 instrument. *In situ* UV-visible measurements were performed using a Hellma all-quartz immersion probe. Electron paramagnetic resonance spectra were measured on a Bruker X-Band EMX spectrometer equipped with an Oxford Instruments

liquid helium cryostat. EPR spectra were typically obtained on 5 mM solutions with a microwave power of 20.5 mW, a modulation frequency of 100 kHz, and a modulation amplitude of 1 G. Cyclic voltammograms were obtained on a CH instruments CHI600E electrochemical workstation using a three component system consisting of a glassy carbon working electrode, a platinum counter electrode, and a silver wire pseudo-reference electrode. Potentials were corrected to Fc/Fc^+ using an internal ferrocene standard.

Crystallographic data for **4** were collected on a Rigaku AFC10K Saturn 944+ CCD-based X-ray diffractometer equipped with a low temperature device and a Micromax-007HF Cu-target micro-focus rotating anode (λ= 1.54187 Å) operated at 1.2 kW power (40 kV, 30 mA). The X-ray intensities were measured at 85(1) K with the detector placed at a distance of 42.00 mm from the crystal. A total of 3859 images were collected with an oscillation width of 1.0° in ω. The exposure time was 1 sec. for the low angle images, 6 sec. for high angle. The integration of the data yielded a total of 72012 reflections to a maximum 2θ value of 136.50° of which 5202 were independent and 4851 were greater than $2\sigma(I)$. The final cell constants were based on the xyz centroids of 15099 reflections above $10\sigma(I)$. Analysis of the data showed negligible decay during data collection; the data were processed with CrystalClear 2.0 and corrected for absorption. The structure was solved and refined with the Bruker SHELXTL (version 2008/4) software package, using the space group P2(1)/n with Z = 4 for the formula $C_{17}H_{35}N_8O_7F_6S_2Fe$. All non-hydrogen atoms were refined anisotropically with the hydrogen atoms placed in idealized positions. Additional details are presented in Table S2 and are given as Supporting Information in a CIF file. The structure is registered with the CCDC under no. 1841320.

Nuclear resonance vibrational spectroscopy (NRVS) data were obtained as described previously[5,6] at beamline 3ID at the Advanced Photon Source (APS) at Argonne National

Laboratory. Samples were loaded in copper sample holders with lucite lids. During data collection, samples were maintained at cryogenic temperatures using a liquid helium-cooled cryostat. Spectra of solid samples were recorded from −50 to +80 meV (hs-{FeNO}^{7}, hs-{FeNO}^{8}) or +90 meV (hs-{FeNO}^{6}) in 0.25 meV steps. Multiple scans were taken, normalized to the intensity of the incident beam, and added together to achieve adequate signal to noise; the final spectra represent averages between 4 and 10 scans. The program Phoenix[5] was used to convert the raw NRVS data to the vibrational density of states (VDOS).

MCD spectra were recorded on a setup consisting of an Oxford SM4000 cryostat and a Jasco J-815 CD spectrometer as described previously.[7,8] The MCD spectra were measured in θ = mdeg and converted to $\Delta\varepsilon$ using the conversion factor $\Delta\varepsilon = \theta / (32980 \cdot cd \cdot B)$, where c is the concentration, d is the path length, and B is the magnetic field strength. For **1-3**, the product cd was substituted by $A_{MCD} / \varepsilon_{UV\text{-}Vis}$ where A_{MCD} is the absorbance of the sample measured by the MCD spectrometer and $\varepsilon_{UV\text{-}Vis}$ is the extinction coefficient. For **5**, A_{MCD} could not be determined due the low absorbance of the sample; in this case, cd was determined from the concentration of the sample and the approximate path length of the sample holder (0.2 cm). Gaussian deconvolution of the spectra was performed using the program PeakFit. VTVH fits were performed as previously described[7] following the method developed by Neese and Solomon.[9]

Mössbauer spectra were recorded on spectrometers from SEECO (Edina, MN). The spectrometer used to record the weak-field spectra is equipped with a Janis SVT-400 variable-temperature cryostat, whereas the spectrometer used to acquire the strong-field spectra is equipped with a Janis 8TMOSS-OM-12SVT variable-temperature cryostat. The quoted isomer shifts are relative to the centroid of the spectrum of α-iron metal at room temperature. Simulations of the Mössbauer spectra were carried out using the WMOSS spectral analysis software from SEECO

(www.wmoss.org; Edina, MN). Some of the simulations are based on the commonly used spin Hamiltonian in which the first three terms describe the electron Zeeman effect and zero field splitting (ZFS) of the electron spin ground state, the fourth term represents the interaction between the electric field gradient and the nuclear quadrupole moment, the fifth term describes the magnetic hyperfine interactions of the electronic spin with the ^{57}Fe nucleus, and the last term represents the ^{57}Fe nuclear Zeeman interaction:

$$\mathbf{H} = \beta \mathbf{S} \bullet \mathbf{g} \bullet \mathbf{B} + D\left(\mathbf{S}_\mathbf{z}^2 - \frac{S(S+1)}{3}\right) + E\left(\mathbf{S}_\mathbf{x}^2 - \mathbf{S}_\mathbf{y}^2\right)$$
$$+ \frac{\mathbf{eQV_{zz}}}{4}\left[\mathbf{I}_\mathbf{z}^2 - \frac{I(I+1)}{3} + \frac{\eta}{3}\left(\mathbf{I}_\mathbf{x}^2 - \mathbf{I}_\mathbf{y}^2\right)\right] + \mathbf{S} \bullet \mathbf{A} \bullet \mathbf{I} - g_n \beta_\mathbf{n} \mathbf{B} \bullet \mathbf{I}$$

X-ray absorption spectra were measured at Stanford Synchrotron Radiation Lightsource, beamline 9-3. Spectra for duplicate samples of hs-{FeNO}^{6}, hs-{FeNO}^{7}, and hs-{FeNO}^{8} were measured in transmission mode using N_2 filled ion chambers. Data for H{FeNO}^{8} were measured as fluorescence excitation spectra using a 100-element Ge monolithic solid-state detector. The output from each detector channel was analyzed and anomalous channels were omitted from the final averaging. The beam was monochromatized using a liquid-nitrogen cooled Si(220) double-crystal monochromator, with harmonic rejection using a vertically collimating, Rh-coated Si mirror. The absorbance spectrum for an Fe foil was measured simultaneously with the sample measurements using an in-line third ion chamber. Spectra were measured with steps of 0.25 eV in the edge region (7092-7142 eV) and then steps of 0.05 Å^{-1} to k=12.8 Å^{-1} (solids) or 11.5 Å^{-1} (solution). Three or four scans were measured for each solid sample; a total of 13 scans were measured for the H{FeNO}^{8} solution. For each sample, successive spectra were compared to confirm that there was no apparent radiation damage.

EXAFS data reduction was accomplished using the EXAFSPAK software.[10] The process began with energy calibration, defining the first inflection point of the Fe foil as 7111.2 eV. Data were then averaged, a linear pre-edge was subtracted, and then a 3-region quartic spline was used to isolate the EXAFS (for the solution data, a shorter 2 region cubic spline was used). XANES spectra were normalized by fitting a single polynomial and scale factor to simultaneously fit the data below the edge and above the edge to tabulated x-ray absorption cross-sections, using the program MBACK.[11]

Theoretical EXAFS amplitude and phase factors were calculated applying FEFF9.6,[12] using one arm of the ligand plus the amine nitrogen and the NO. Non-hydrogen scattering paths with a curved-wave amplitude >5% were retained, giving a total of 55 ligand paths for the ligand from the hs-$\{FeNO\}^6$ complex and 44 ligand paths for the ligand from the less-symmetric hs-$\{FeNO\}^7$ complex. FEFF calculations were performed for Fe-N-O angles ranging from 130° to 180° in steps of 10°, with 4 scattering pathways retained.

The one-electron reduction of the hs-$\{FeNO\}^6$ complex causes a significant distortion in the ligand structure, with a much longer Fe-N_{amine} distance and significantly longer Fe-(C,N) outer-shell scattering. These differences can be seen in the Fourier transform of the FEFF-simulated EXAFS for the two different ligands (Figure S1). Because of this difference, the choice of ligand had a small effect on the resulting fit. The biggest effect was seen in the fitted Debye-Waller factors; fits of the hs-$\{FeNO\}^6$ complex using the hs-$\{FeNO\}^7$ ligand geometry gave a smaller σ^2(Fe-N_{ligand}) value and a much larger σ^2(Fe-N_{NO}) value, while fits of the hs-$\{FeNO\}^7$ complex using the hs-$\{FeNO\}^6$ ligand geometry gave an unusually large σ^2(Fe-N_{ligand}) value and a somewhat smaller σ^2(Fe-N_{NO}) value, with little change in apparent distances for either case. The fits for the hs-$\{FeNO\}^8$ and H$\{FeNO\}^8$ compounds show behavior similar to that for the hs-

{FeNO}^{7} complex, suggesting that they have a similar ligand structure, as expected. The hs-{FeNO}^{7} ligand simulation was therefore used for the fits of the hs-{FeNO}^{8} and H{FeNO}^{8} data.

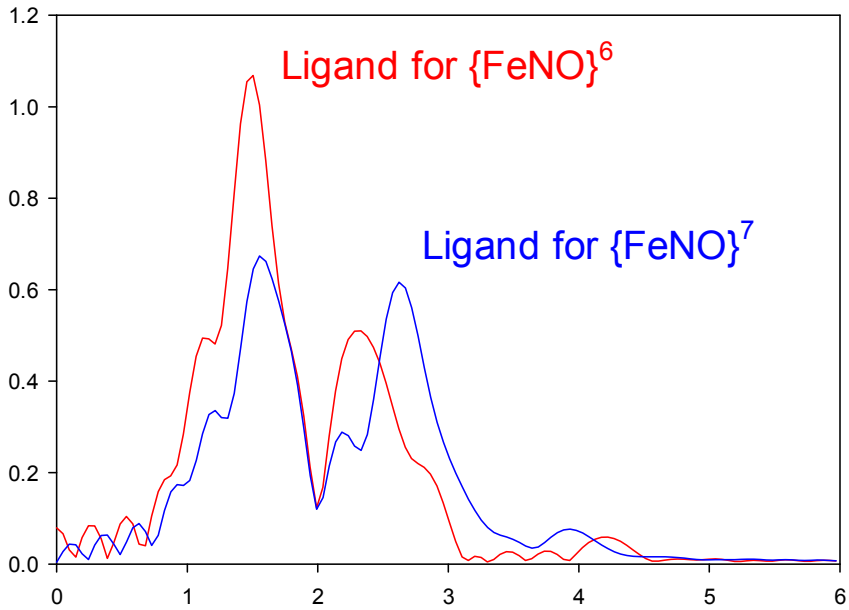

Figure S1. Fourier transforms of the k^3 weighted simulated EXAFS for the ligand geometries obtained from the crystal structures of the hs-{FeNO}^{6} and hs-{FeNO}^{7} complexes.

For the fits reported in the manuscript, the threshold energy, E_0, was set to 7119 eV, a value found in previous fits[13] of Fe EXAFS to give accurate structural parameters. Additional fits in which E_0 was allowed to vary gave slightly (~0.02 Å) different distances and no change in the relative fit quality. The fitting began with a minimal nearest-neighbor fit consisting of two shells: 4 N atoms at ~2 Å and 1 N atom at ~1.7 Å. In no case was it possible to account for the nearest neighbor scattering without including both shells. The fitted Fe-N distances from this simple model provided a baseline against which to compare the more complicated multiple-scattering fits. The final Fe-N distances reported in the manuscript agree with those from the simple two-shell fits to within 0.05 Å, and reproduce the trends seen in the simpler model.

The fits reported in the manuscript used 4 variable parameters: two distances, r(Fe-N_{ligand}) and r(Fe-N_{NO}), and two Debye-Waller factors, σ^2(Fe-N_{ligand}) and σ^2(Fe-N_{NO}), with the remaining

structural parameters fixed by assuming a rigid ligand. For each sample, a fit using only the ligand gave a mean-square deviation that was 50-100% higher than a fit that included the ligand and the NO (as expected from the simple two-shell fits). Fits were attempted by varying the Fe-N-O angle in the 130-180° interval (in steps of 10°), and recalculating each of the different NO-dependent scattering parameters for each angle. The fits showed relatively modest sensitivity to the Fe-N-O angle, reflecting the complex interplay between ligand and NO outer-shell scattering; the estimated uncertainty is no better than ±10°, and probably worse for H{FeNO}^{8} due to the shorter *k* range for the latter. For hs-{FeNO}^{6} and H{FeNO}^{8}, the best fits were found with a linear Fe-N-O unit, while for hs-{FeNO}^{7} and hs-{FeNO}^{8}, a bent Fe-N-O unit gave a somewhat better fit. In addition to giving worse fits, attempts to fit the data for the hs-{FeNO}^{6} and H{FeNO}^{8} complexes using a bent Fe-N-O unit gave unreasonable σ^2(Fe-N_{NO}) values (too small for hs-{FeNO}^{6} and too large for H{FeNO}^{8}). The k^3 weighted EXAFS for the data and the fits, and the Fourier transforms of these data are shown in Figures S2 and S3.

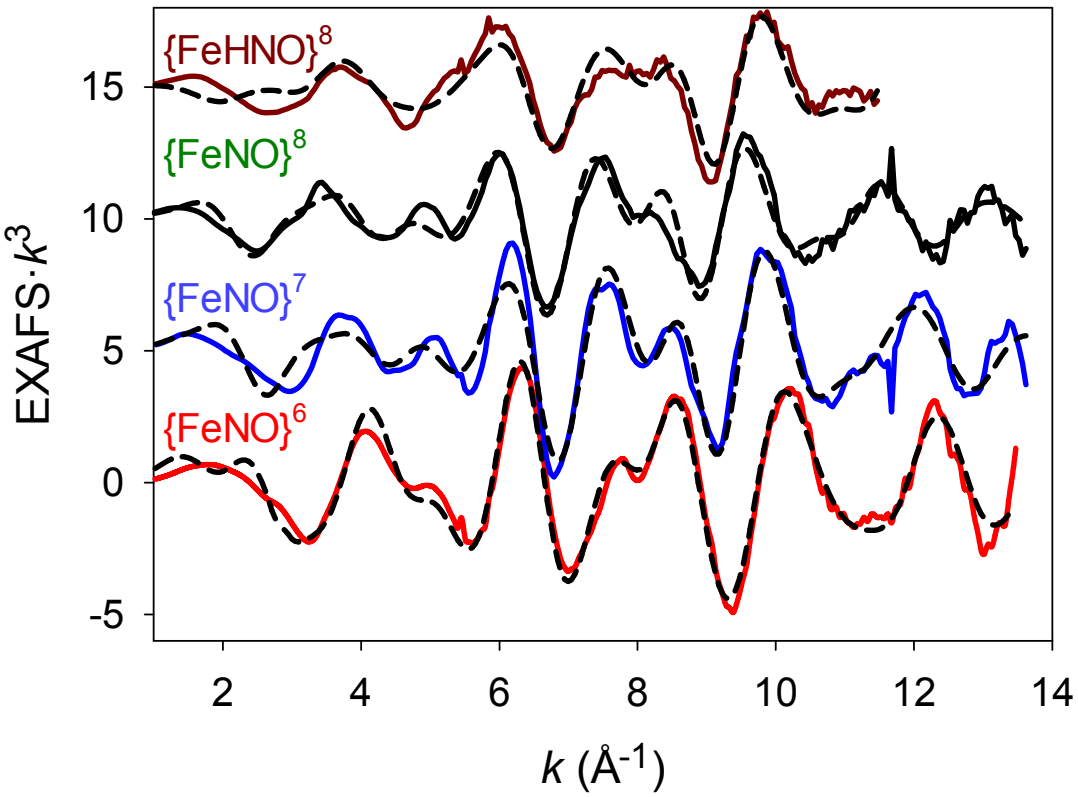

Figure S2. The k^3 weighted EXAFS for the data (solid colored lines) and the fits (black dashed lines). Plots for hs-{FeNO}^{7}, hs-{FeNO}^{8}, and H{FeNO}^{8} are offset vertically for clarity.

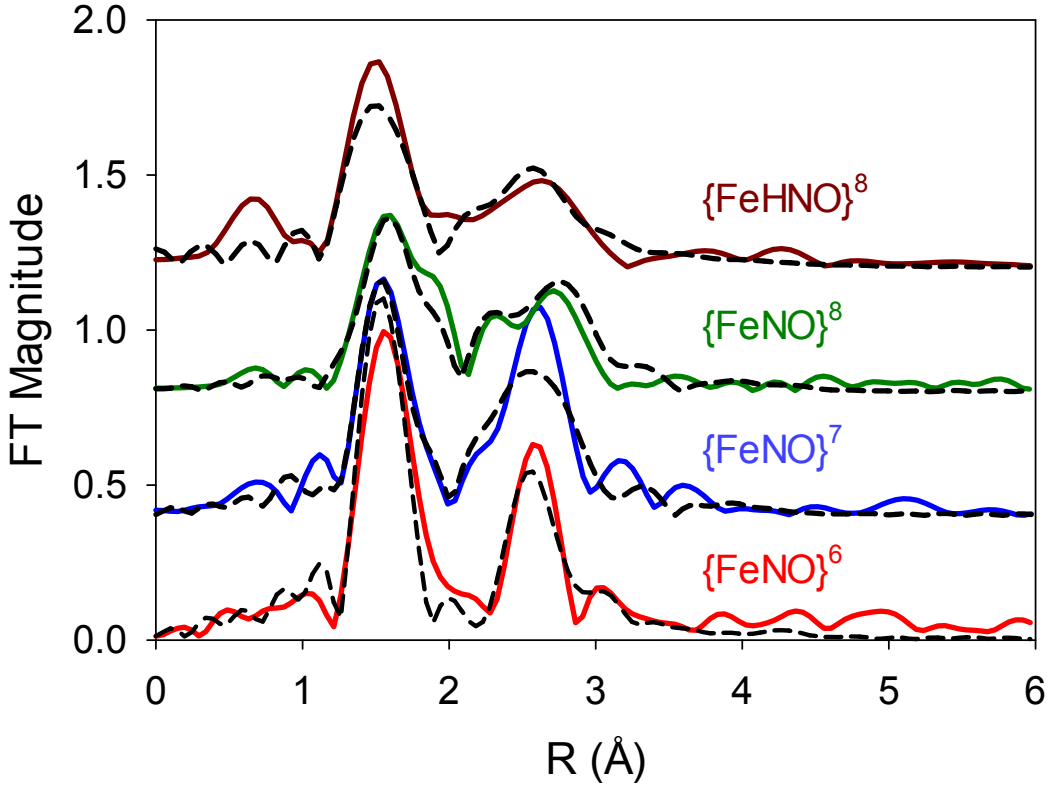

Figure S3. Fourier transforms of the k^3 weighted EXAFS data shown in Figure S2. For each sample, the FT of the data (solid colored lines) and the fit (black dashed lines) were calculated over the same k-range (k=1-k_{max}). Plots for hs-{FeNO}^{7}, hs-{FeNO}^{8}, and H{FeNO}^{8} are offset vertically for clarity. The shorter available k range for H{FeNO}^{8} compared to the other samples gives a slightly broader peak.

DFT Calculations

All geometry optimizations and frequency calculations except those used for the QCC-NCA fitting procedure were performed with the ORCA program package[14] (version 2.9, and version 4.0 in the case of the ligand-protonated species) at the TPSS/def2-TZVP(-f) level, employing the RI approximation with the def2-TZV/J auxiliary basis set. For the ligand-protonated species, the CPCM solvent model (with acetonitrile) was used. The structures were confirmed to be minima based on the absence of imaginary frequencies. In the case of the ligand-protonated species, several low-energy (less than 120 cm^{-1}) imaginary frequencies associated with large-scale

motions of the ligand periphery were observed. The TPSS-optimized structures were further used to calculate the zero field splitting (ZFS) parameters, ^{57}Fe hyperfine coupling constants, electric field gradients, and the Mössbauer parameters. Mössbauer parameters were calculated using the B3LYP functional and the basis sets CP(PPP) on Fe, TZVP on N and O, and SV(P) on C and H. Isomer shifts (δ) were calculated using the correlation between ρ(0) (the electron density at the iron nucleus) and δ reported in the literature.[15] ZFS calculations were performed with the TZVP basis set and the indicated functionals.

QCC-NCA Fitting

Geometry optimizations and frequency calculations for the QCC-NCA fitting procedure were performed with the Gaussian09 program package[16] using the TPSS functional and TZVP basis set. The force constants were transformed to internal coordinates and extracted using a modified version of the program Redong[17], and a modified NCA program[18] based on QCPE 576[19] was used to calculate the NRVS VDOS. The data were then fitted by adjusting a minimal set of force constants (in the spirit of the QCC-NCA approach)[20] to reproduce the vibrations of the Fe-N-O unit in complexes **1** – **3** (see text).

SI Figures Section 2.1

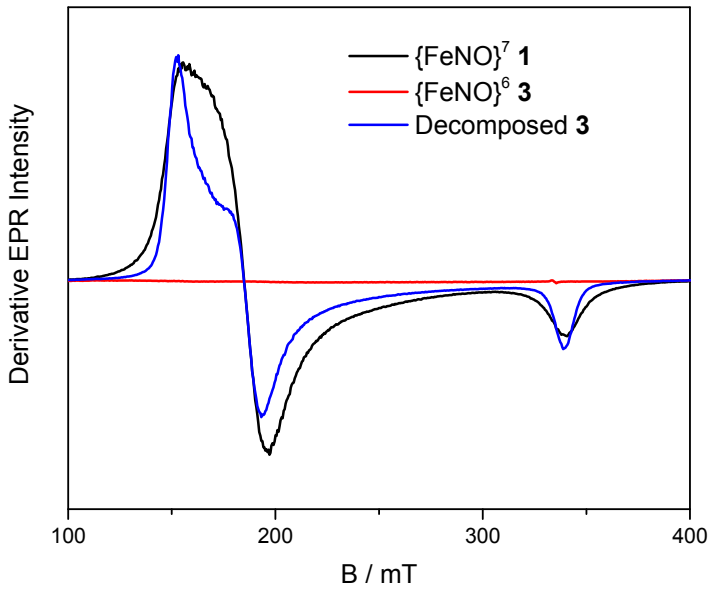

Figure S4. EPR spectra (recorded at 4 K) of **1** (black), **3** (red), and the product of the decomposition of **3** (blue) after 25 minutes at room temperature in CH_3CN.

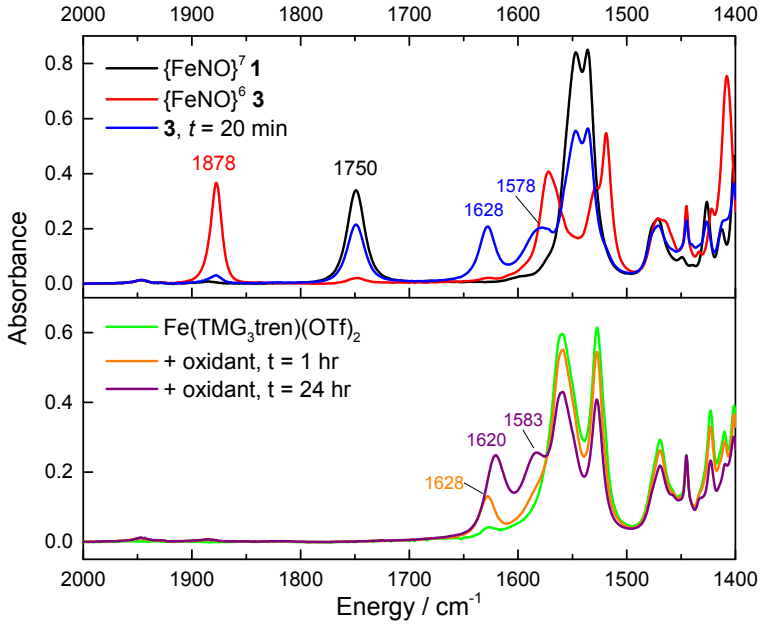

Figure S5. Solution IR spectra showing the product of the decomposition of **3** at room temperature (top). Spectra showing the decomposition of the ferrous precursor $[Fe(TMG_3tren)](OTf)_2$ upon oxidation with the thianthrene radical cation are shown for comparison in the bottom panel. Note that previous studies have demonstrated that in the absence of an axial ligand, ferric TMG_3tren complexes are unstable.[21,22]

Table S1. Comparison of experimental and DFT-calculated (TPSS/def2-TZVP(-f), except where noted) geometric and spectroscopic parameters for **1-3**.[3]

	{FeNO}^{6} Expt.	**{FeNO}^{6} DFT**	**{FeNO}^{7} Expt.**	**{FeNO}^{7} DFT**	**{FeNO}^{8} Expt.**	**{FeNO}^{8} DFT**
Fe-N(O) (Å)	1.680	1.666	1.748	1.721	--	1.694
N-O (Å)	1.142	1.151	1.154	1.177	--	1.202
Fe-N-O (°)	180	180	168	154	--	159
Fe-N_{amine} (Å)	2.020	2.042	2.251	2.222	--	2.360
Avg. Fe-N_{guan} (Å)	1.966	2.008	2.037	2.071	--	2.160
δ (mm/s)[c]	0.06	0.07	0.48	0.38	0.84	0.72
ΔE_Q (mm/s)[c]	0.48	0.40	–1.42	–1.69	-2.78	2.13
ν(NO) (cm^{-1})	1878[a,b]	1874	1730-1745[a] 1750[b]	1714	1618[b]	1628

[a] Solid state (KBr pellet) [b] In CD_3CN solution [c] Calculated with the B3LYP functional and basis sets CP(PPP) (Fe), TZVP (N/O), and SV(P) (C, H).

SI Figures and Tables Section 2.2

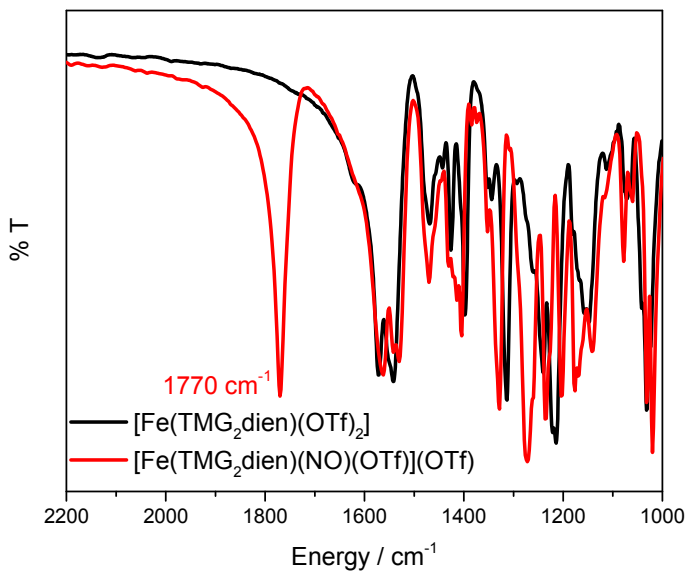

Figure S6. (a) FT-IR spectrum (KBr pellet) of [Fe(TMG$_2$dien)(NO)(OTf)](OTf) (**4**) and of the corresponding ferrous precursor.

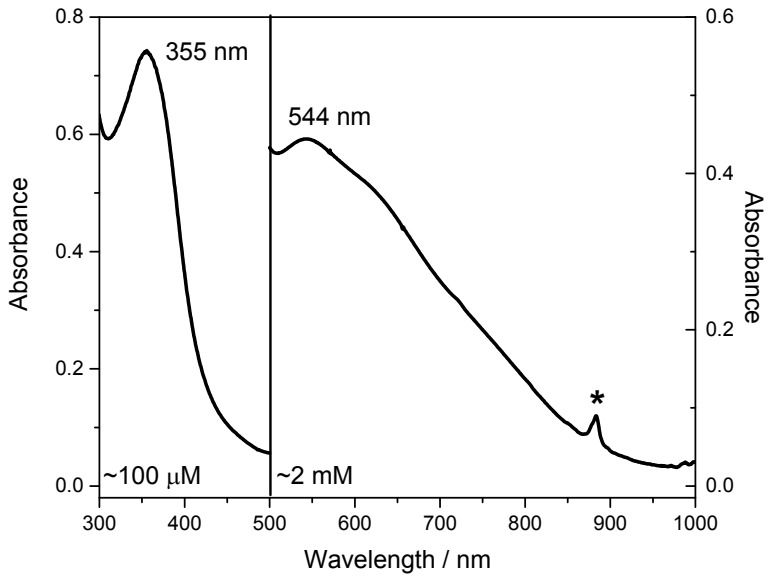

Figure S7. UV-Visible spectrum of [Fe(TMG$_2$dien)(NO)(OTf)](OTf) (**4**) at low (left) and high (right) concentration in dichloromethane. The sharp peak denoted by the asterisk arises from an instrumental artifact.

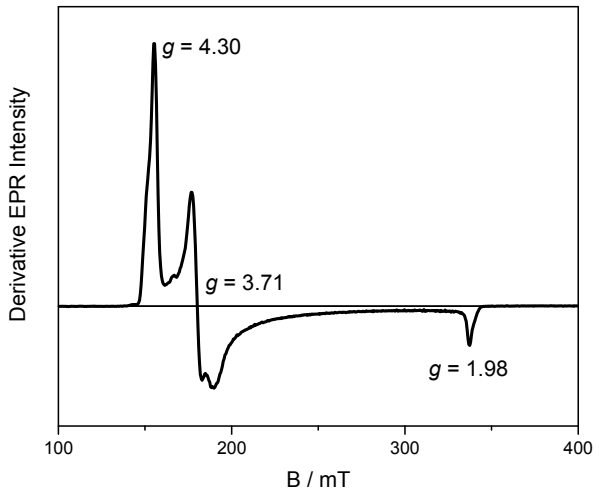

Figure S8. X-band EPR spectrum of [Fe(TMG$_2$dien)(NO)(OTf)](OTf) (**4**) recorded at 4.2 K in frozen 1:1 propionitrile:butyronitrile solution.

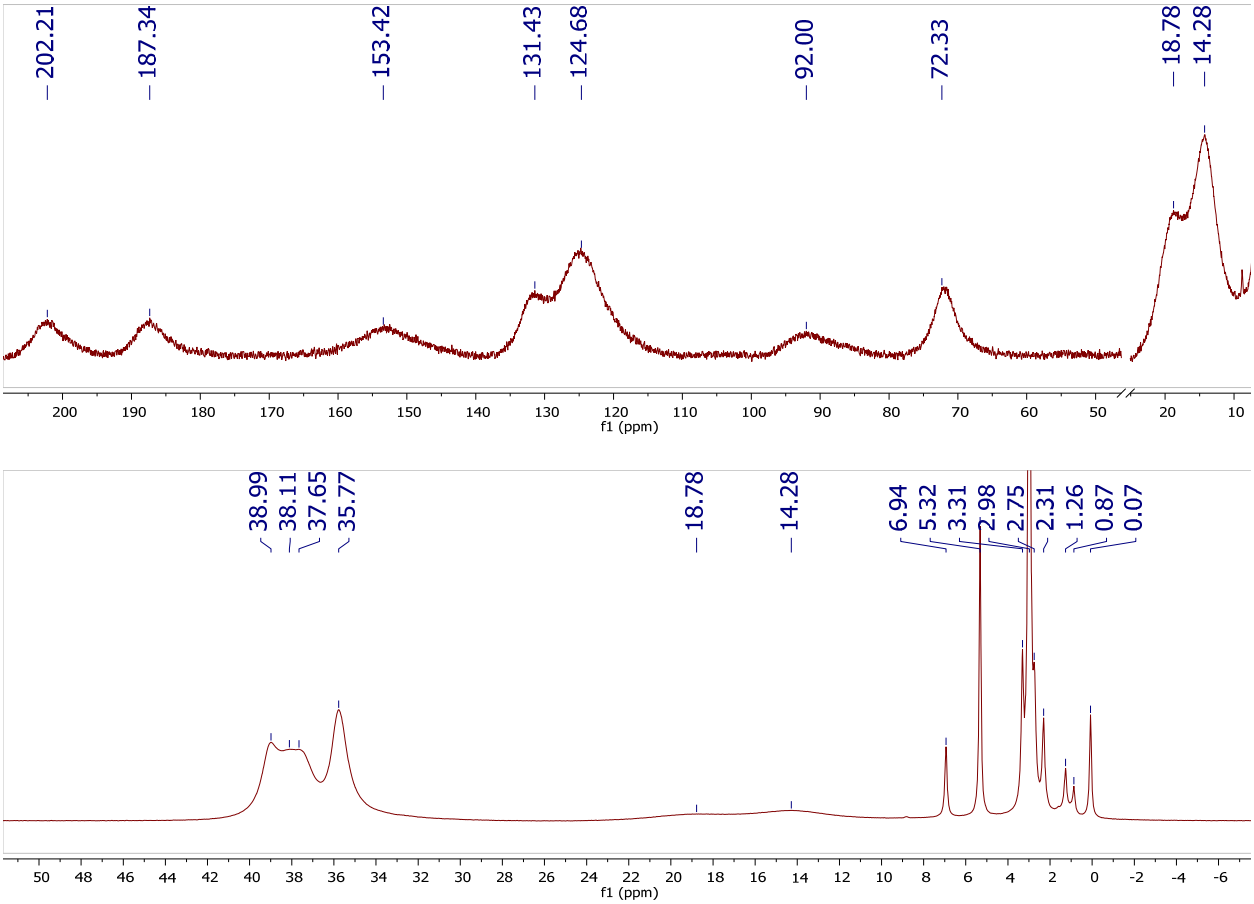

Figure S9. ^{1}H-NMR spectrum of [Fe(TMG$_2$dien)(NO)(OTf)](OTf) (**4**) in CD_2Cl_2. The signals are unusually broad, which we hypothesize is due to the formation of a paramagnetic precipitate resulting from decomposition (most likely adventitious oxidation).

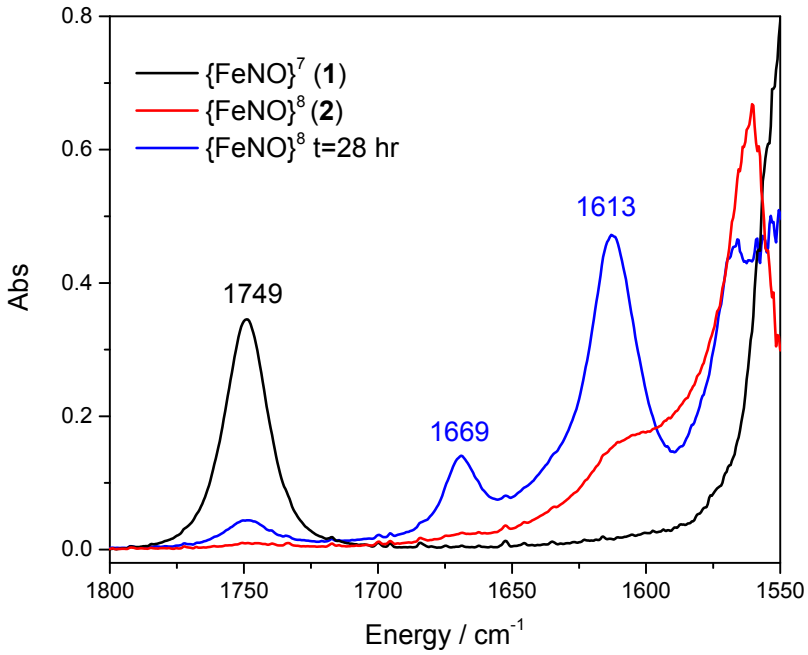

Figure S10. Solution IR spectrum showing the decomposition of **2** at room temperature in CH_3CN.

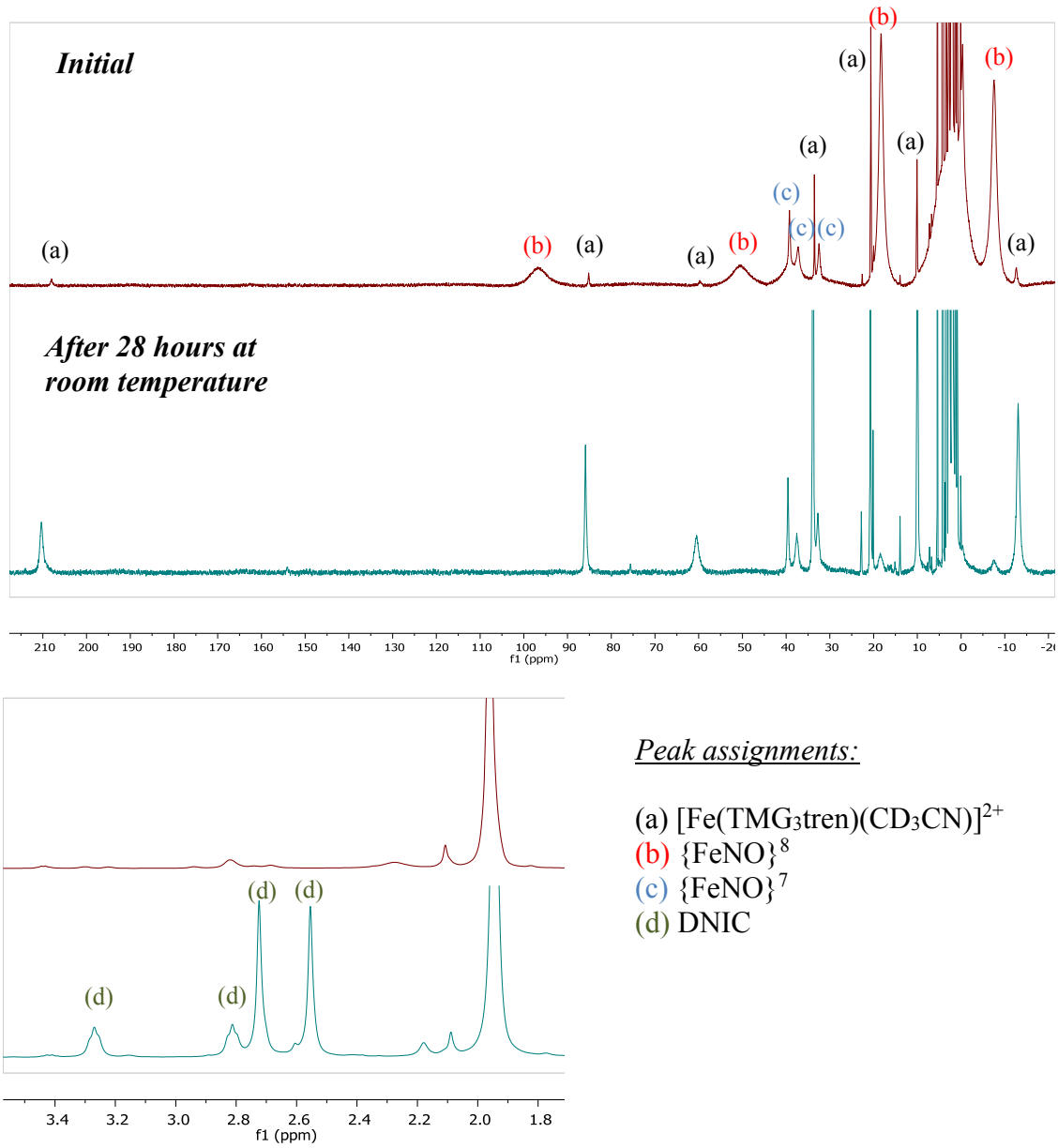

Figure S11. ^{1}H-NMR spectra showing the decomposition of the hs-{FeNO}^{8} complex **2** at room temperature in CD_3CN. The initial hs-{FeNO}^{8} complex (b) is contaminated with small amounts of the hs-{FeNO}^{7} complex (c) and the ferrous complex $[Fe(TMG_3tren)(CD_3CN)]^{2+}$ (a). Upon stirring at room temperature overnight, the hs-{FeNO}^{8} complex decomposes to produce additional ferrous complex and a new diamagnetic species (d) which we tentatively assign to the DNIC (as indicated by IR spectroscopy, see Figure S10).

Table S2. Crystal data and structure refinement for [Fe(TMG$_2$dien)(NO)(OTf)](OTf) (**4**)

Empirical formula	$C_{17}H_{35}F_6FeN_8O_7S_2$	
Formula weight	697.50	
Temperature	85(2) K	
Wavelength	1.54178 Å	
Crystal system	Monoclinic	
Space Group	P2(1)/n	
Unit cell dimensions	a = 11.6666(2) Å	α = 90 °
	b = 8.2513(2) Å	β = 90.93.577(7) °
	c = 30.021(2) Å	γ = 90 °
Volume	2884.3(2) Å^3	
Z, calculated density	4, 1.606 Mg/m^3	
Absorption coefficient	6.378 mm^{-1}	
F(0,0,0)	1444	
Crystal size	0.16 x 0.02 x 0.02 mm	
Theta range for data collection	3.99° to 69.25°	
Limiting indices	$-13 \leq h \leq 13$, $-9 \leq k \leq 9$, $-36 \leq l \leq 36$	
Reflections collected / unique	72012 / 5202 [R(int) = 0.1013]	
Completeness to theta = 68.25	98.8%	
Absorption correction	Semi-empirical from equivalents	
Max. and min. transmission	1.00000 and 0.50020	
Refinement method	Full-matrix least-squares on F^2	
Data / restraints/parameters	5202 / 0 / 379	
Goodness of fit on F^2	1.140	
Final R indices [I>2sigma(I)]	R1 = 0.0435, wR2 = 0.1207	
R indices (all data)	R1 = 0.0458, wR2 = 0.1255	
Largest diff. peak and hole	0.469 and -0.631 e.A^{-3}	

SI Figures and Tables Section 2.3

Table S3. DFT-calculated *D* (top) and *E/D* (middle) values in cm^{-1} for TMG_3tren complexes (TPSS/def2-TZVP(-f) optimized structures), using the indicated functionals and the TZVP basis set. Values were also calculated with an extended CP(PPP) basis set on Fe (given in parentheses). DFT-calculated ^{57}Fe hyperfine coupling constants (*A*) in MHz (bottom) for TMG_3tren complexes were obtained with the TPSS/TZVP combination.

Compound	Expt. *D* Value	BP86	PBE	TPSS	B3LYP	PBE0	TPSSh
Fe(IV)=O	5.0 [22]	2.8 (2.7)	2.8 (2.8)	2.7 (2.6)	3.3 (-5.1)	3.0 (3.3)	2.8 (2.8)
hs-{FeNO}^{6}	27 (this work)	16.6 (16.6)	16.9 (16.8)	15.7 (15.6)	--	--	--
hs-{FeNO}^{7}	6.0 [2] (this work)	4.6 (4.5)	4.6 (4.5)	4.2 (4.2)	2.8 (9.1)	2.4 (-7.8)	2.4 (-2.8)
hs-{FeNO}^{8}	17 (this work)	-4.8 (-4.5)	-4.9 (-4.6)	-4.2 (-4.0)	--	--	--

Compound	Expt. *E/D*	BP86	PBE	TPSS	B3LYP	PBE0	TPSSh
Fe(IV)=O	0.020 [22]	0.043 (0.001)	0.001 (0.001)	0.001 (0.001)	0.015 (0.297)	0.001 (0.146)	0.002 (0.022)
hs-{FeNO}^{6}	0.06 (this work)	0.0001 (0.0001)	0.0001 (0.0001)	0.0001 (0.0001)	--	--	--
hs-{FeNO}^{7}	0.063 [2]	0.048 (0.001)	0.095 (0.001)	0.094 (0.001)	0.088 (0.214)	0.098 (0.157)	0.080 (0.084)
hs-{FeNO}^{8}	0.06 (this work)	0.091 (0.106)	0.092 (0.107)	0.108 (0.127)	--	--	--

Compound	*A*(x)	*A*(y)	*A*(z)
hs-{FeNO}^{6}	-6.9254	-6.9752	-45.4792
hs-{FeNO}^{7}	-19.8007	-21.2784	-30.0146
hs-{FeNO}^{8}	-1.882	-28.6206	-31.6127

Table S4. Euler angles for the rotation of the DFT-calculated electric field gradient (EFG) and ^{57}Fe hyperfine coupling (HFC) tensors onto the zero-field splitting (ZFS) tensor, taken from the BP86/TZVP calculations (see Table S3; for TPSS/def2-TZVP(-f) optimized structures).

		Euler Angles			
		Initial z-axis	**New y-axis**	**New z-axis**	**Comments**
hs-{FeNO}^{6}	EFG → ZFS	118.3	180	0	The ZFS z-component points along the Fe-N(O) bond, while the EFG and HFC z-components point in opposite direction. All are collinear with the Fe-N(O) bond.
	HFC → ZFS	134.6	180	0	
hs-{FeNO}^{7}	EFG → ZFS	143	180	0	The ZFS and HFC z-components point along the Fe-N(O) bond, while the EFG z-component points in opposite direction. All are collinear with the Fe-N(O) bond.
	HFC → ZFS	121.9	0	0	
hs-{FeNO}^{8}	EFG → ZFS	68.5	-107	8.5	The ZFS z-component is nearly perpendicular to the Fe-N(O) bond. The EFG z-component points away from the Fe-NO bond and is no longer fully collinear with the Fe-N(O) axis (angle: 150°).
	HFC → ZFS	1.1	-7.3	0.5	

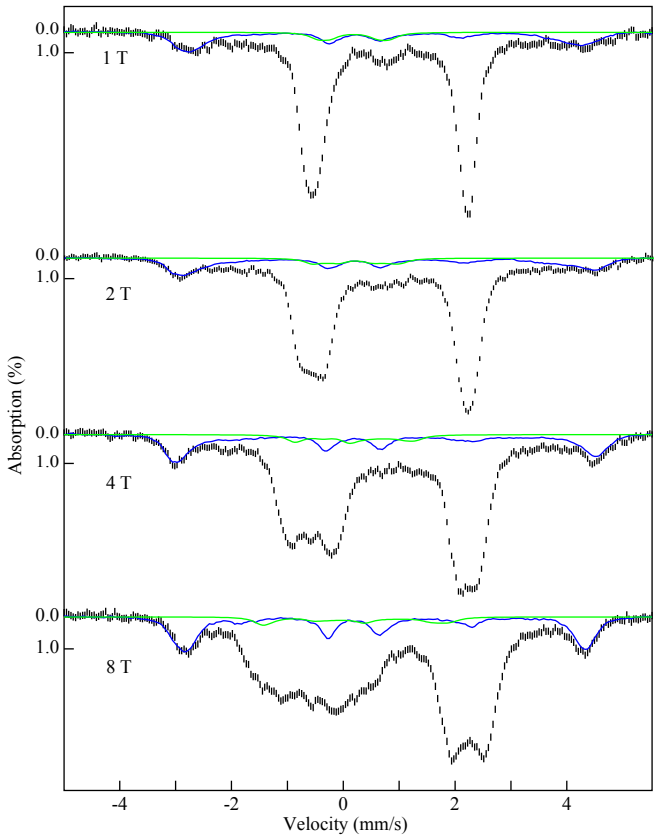

Figure S12. 4.2 K/variable-field Mössbauer spectra of a sample containing a 5 mM solution of the hs-$\{FeNO\}^8$ complex **3** in 1:1 propionitrile:butyronitrile. The blue lines are the experimental spectra of the hs-$\{FeNO\}^7$ complex **1** recorded under identical conditions and scaled to 16% of total intensity. The green lines are the simulations of an impurity (likely to be an $\{Fe(NO)_2\}^{10}$ species) with δ = 0.19 mm/s, ΔE_Q = 1.06 mm/s, η = 0, and assuming a diamagnetic ground state and the slow relaxation limit.

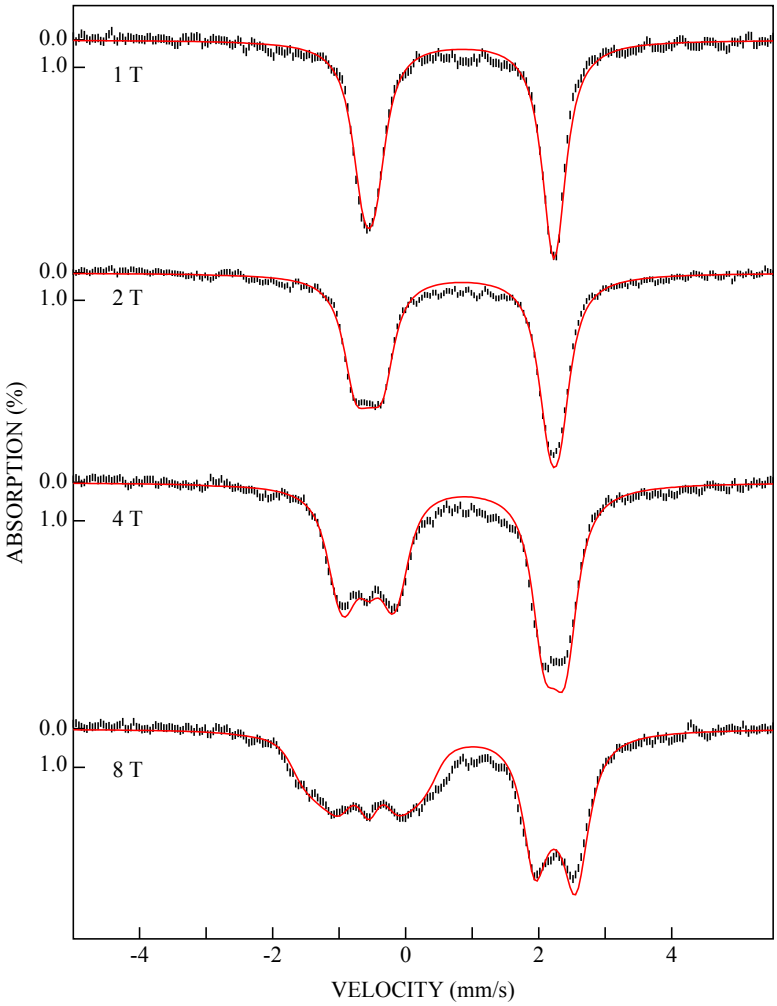

Figure S13. 4.2 K/variable-field Mössbauer spectra of a sample containing a 5 mM solution of the hs-{FeNO}^{8} complex **3** in 1:1 propionitrile:butyronitrile. The experimental spectra are the same as shown in Figure 4B in the main text. The red lines are spin Hamiltonian simulations of the hs-{FeNO}^{8} complex with parameters given in Table S5 (Fit B) using a positive ΔE_Q with inclusion of Euler angles, and assuming the slow relaxation limit (80% of total intensity). In this simulation, the principle axis frame of the EFG (x,y,z) tensor was rotated to (y,z,x).

Table S5. Comparison of hs-{FeNO}^{8} experimental and DFT-calculated Mössbauer parameters, all with respect to an $S = 1$ spin-coupled system.

	D (cm^{-1})	E/D	$\mathbf{A}/g_n\beta_n$ (T)	ΔE_Q (mm/s)	α ,β,γ [a] (°)	η	δ (mm/s)
Fit A [b]	17	0.06	-17.6, -8.5, -23.3	-2.78	0, 0, 0	1.0	0.84
Fit B	17	0.06	-18.0, -9.0, -20.0	2.78	90, 90, 0	-0.3	0.84
DFT[c]	-4.6	0.095	-2.2, -21.5, -24.1	2.13	69, 106, 8.5	0.3	0.72

[a] The convention of Euler angle rotations are as follows: α represents the rotation around the z axis; β represents the rotation around the new x axis; γ represents the rotation around the new z axis. [b] The parameters reported in the main text. [c] The **A** tensor was calculated by taking the calculated, un-scaled A_{iso} = -15.8 T and adding spin-dipolar and spin-orbital terms from DFT calculations.

Section 2.5 SI Figures and Tables

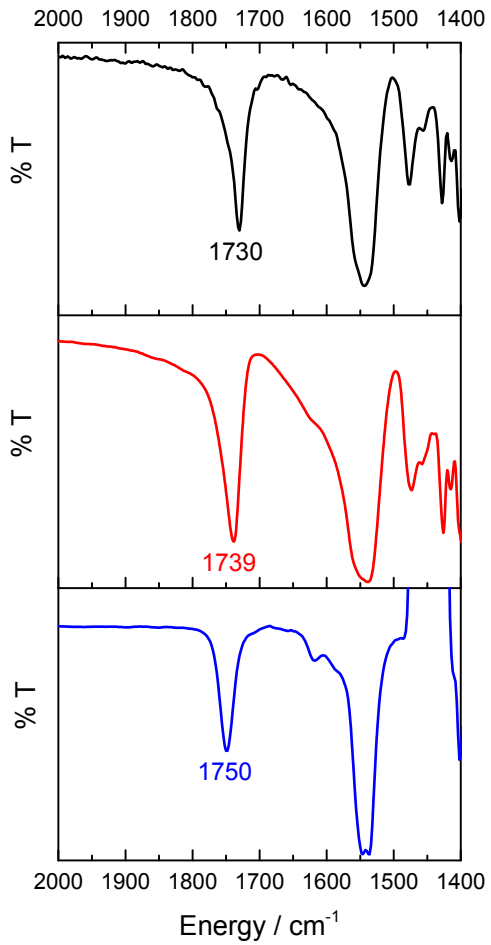

Figure S14. IR spectra of $[Fe(TMG_3tren)(NO)]^{2+}$ (**1**) under different conditions showing variation in the observed N-O stretching frequency. (Top) $[Fe(TMG_3tren)(NO)](OTf)_2$ powder sample in a KBr matrix. (Middle) $[Fe(TMG_3tren)(NO)](BF_4)_2$ powder sample in a KBr matrix. (Bottom) $[Fe(TMG_3tren)(NO)](OTf)_2$ in propionitrile solution. In all cases, dissolved samples show an N-O stretch at 1750 cm^{-1}.

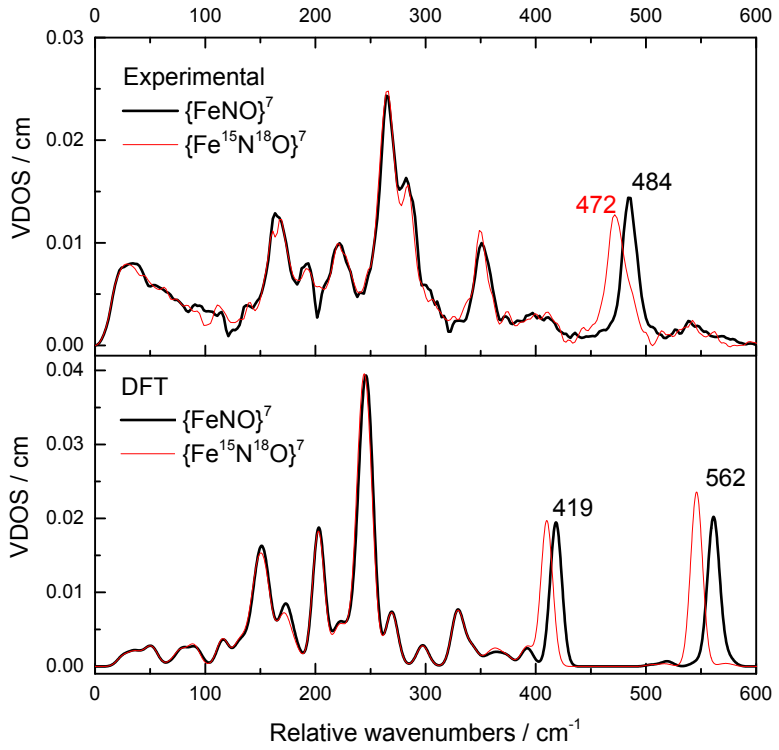

Figure S15. Experimental NRVS VDOS data (top) and DFT (TPSS/TZVP) predicted spectrum (bottom) for [^{57}Fe(TMG$_3$tren)(NO)](BF$_4$)$_2$ (black) and [^{57}Fe(TMG$_3$tren)(^{15}N^{18}O)](BF$_4$)$_2$ (red).

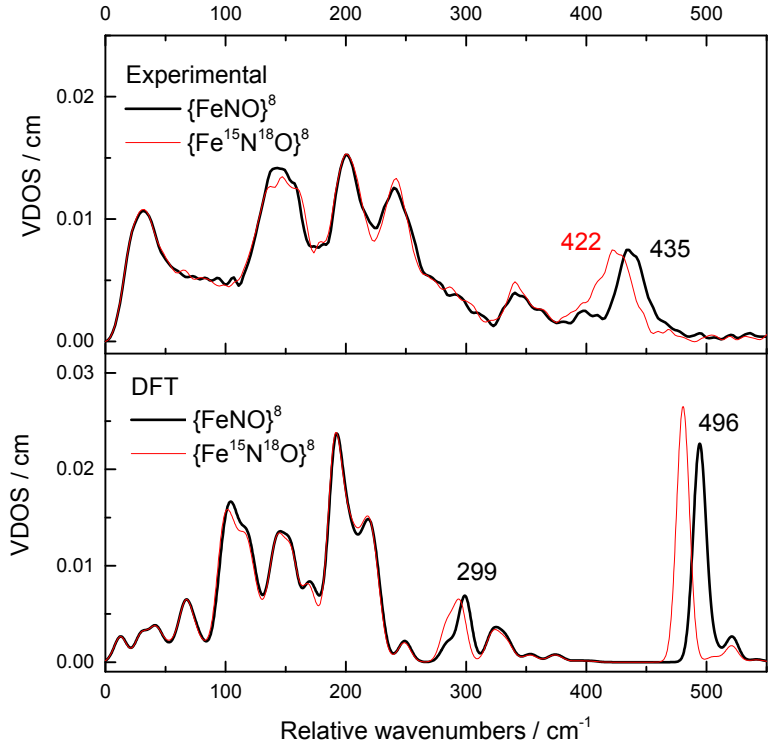

Figure 16. Experimental NRVS VDOS data (top) and DFT (TPSS/TZVP) predicted spectrum (bottom) for [^{57}Fe(TMG$_3$tren)(NO)](BF$_4$) (black) and [^{57}Fe(TMG$_3$tren)(^{15}N^{18}O)](BF$_4$) (red).

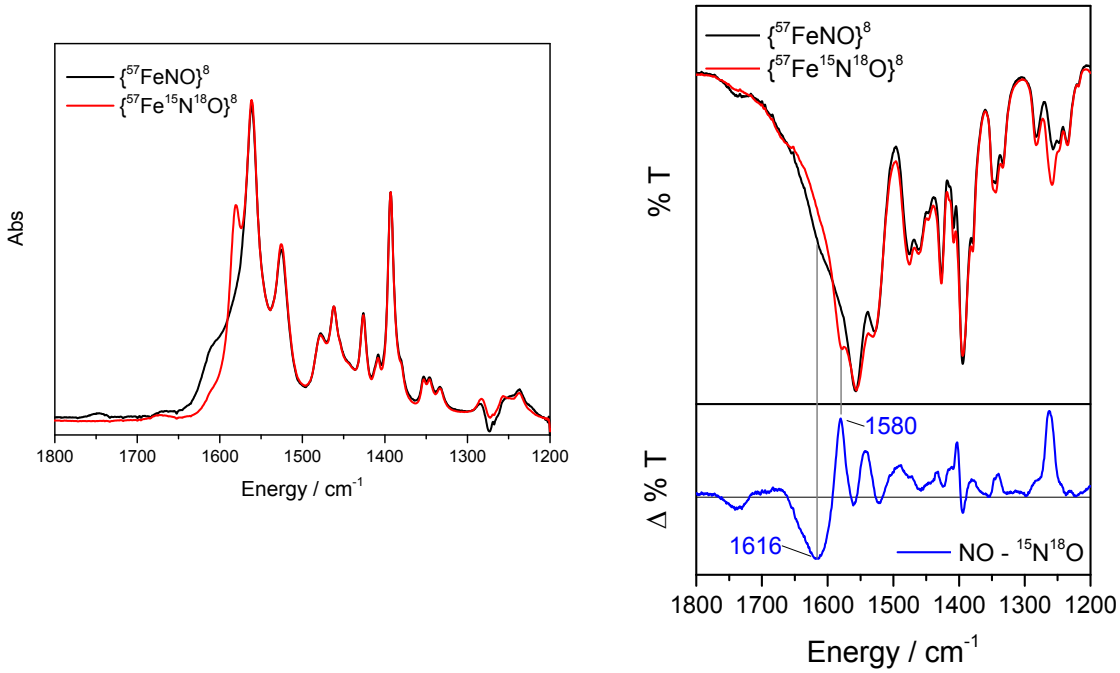

Figure S17. Solution (left) and solid state (KBr, right) IR data for [^{57}Fe(TMG$_3$tren)(NO)](BF$_4$) (black: natural abundance NO; red: ^{15}N^{18}O); the latter includes a difference spectrum (blue). Note that the isotope shift upon ^{15}N^{18}O labeling is much too small compared to what would be expected from a harmonic oscillator model (~38 cm^{-1}, as compared to the shift of 72 cm^{-1} predicted by the harmonic oscillator model). Also note that the N-O and ^{15}N-O stretches appear at 1618 cm^{-1} and 1586 cm^{-1}, respectively, in CD$_3$CN solution,[2] corresponding to an isotope shift of 32 cm^{-1}, which is close to the 29 cm^{-1} shift predicted by the harmonic oscillator model for the ^{15}NO case. The QCC-NCA simulations give an explanation for this unusual observation, without being able to capture the effect quantitatively. As shown in Table 4 in the paper, the N-O stretch is listed as 1594/(1565) cm^{-1} for the QCC-NCA result for the hs-{Fe^{15}NO}^{8} complex. This is because the N-O stretch is mixed with guanidine vibrations in the QCC-NCA simulations for the ^{15}NO case (which is not observed in the experimental IR data). Experimentally, this effect is much more pronounced in the ^{15}N^{18}O-labeled complex, leading to the greatly diminished apparent isotope shift in the IR data of this isotopomer. In the QCC-NCA simulations for the ^{15}N^{18}O complex, there is no single N-O stretch left, but instead, there are four modes of primary guanidine character that acquire some N-O stretching character (one of them is predicted around 1578 cm^{-1}; the lowest energy mode is located at 1540 cm^{-1}). This qualitatively explains our observations: the diminished isotope shift in the ^{15}N^{18}O compound is due to strong mixing of the N-O stretch with several guanidine modes, leading to the loss of a single IR band that can be identified with the N-O stretching vibration in the ^{15}N^{18}O case.

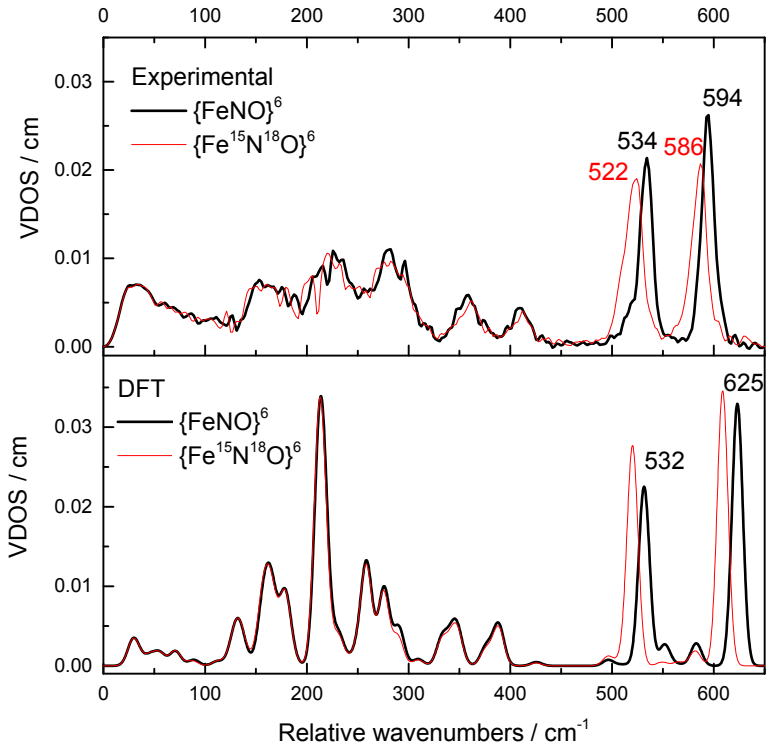

Figure S18. Experimental NRVS VDOS data (top) and DFT (TPSS/TZVP) predicted spectrum (bottom) for [^{57}Fe(TMG$_3$tren)(NO)](BF$_4$)$_3$ (black) and [^{57}Fe(TMG$_3$tren)(^{15}N^{18}O)](BF$_4$)$_3$ (red).

SI Figures and Tables Section 2.6

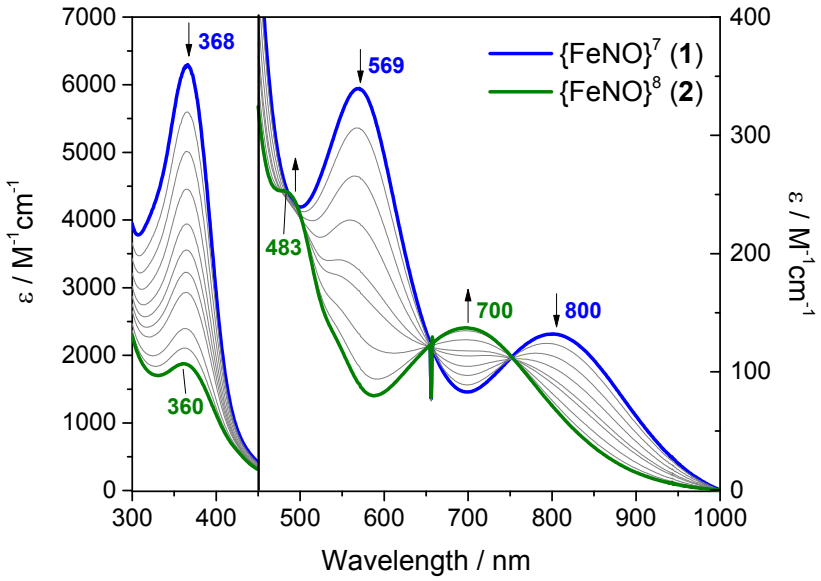

Figure S19. UV-Visible spectroscopy showing the bulk electrolysis of **1** to **2** at high and low concentration in CH_3CN. In experiments performed after our original report,[2] we determined that in the previously reported spectrum, the conversion of **1** to **2** was incomplete.

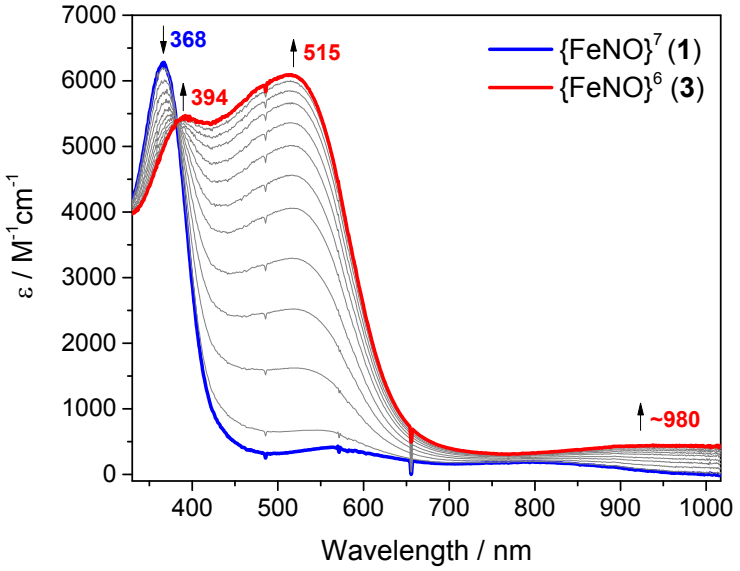

Figure S20. UV-Visible spectroelectrochemistry showing the conversion of **1** to **3** in CH_3CN.[3]

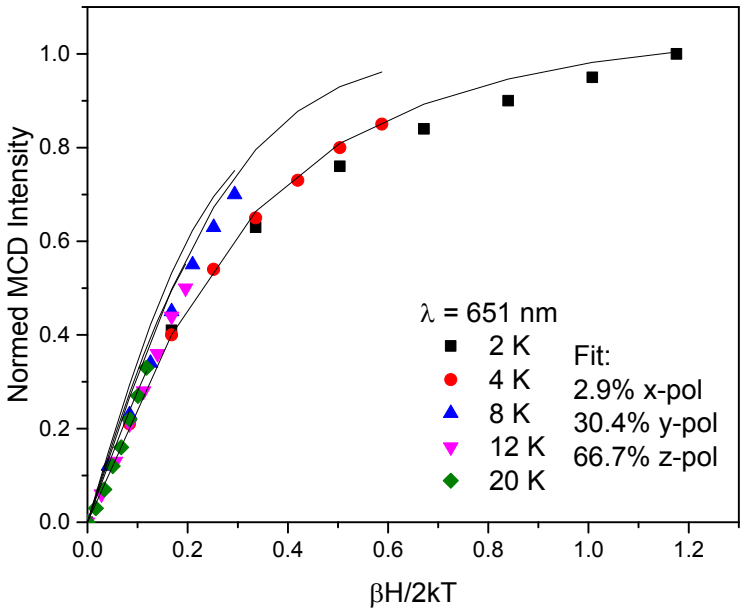

Figure S21. Magnetic saturation curves for band 2 of complex **1**. A satisfactory fit could not be obtained for these data, likely due to the low intensity of this feature and its strong overlap with band 3.

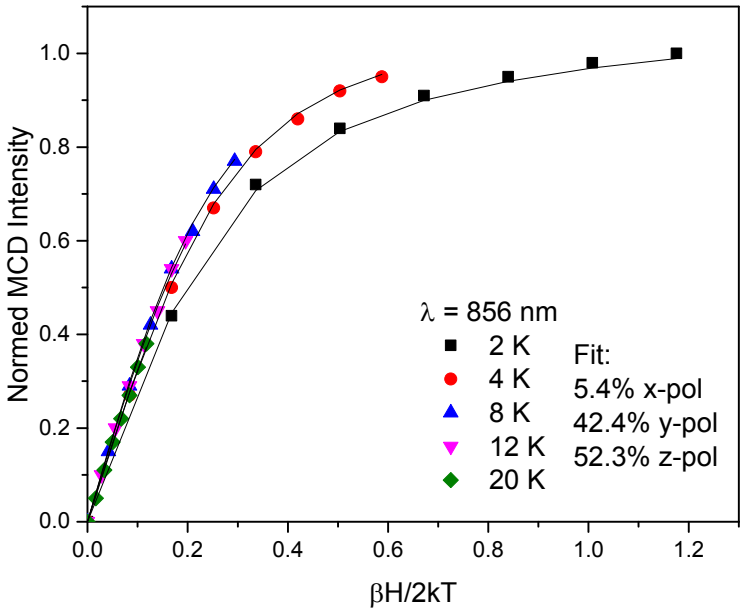

Figure S22. Magnetic saturation curves for the MCD feature at 856 nm (band 1) of complex **1**.

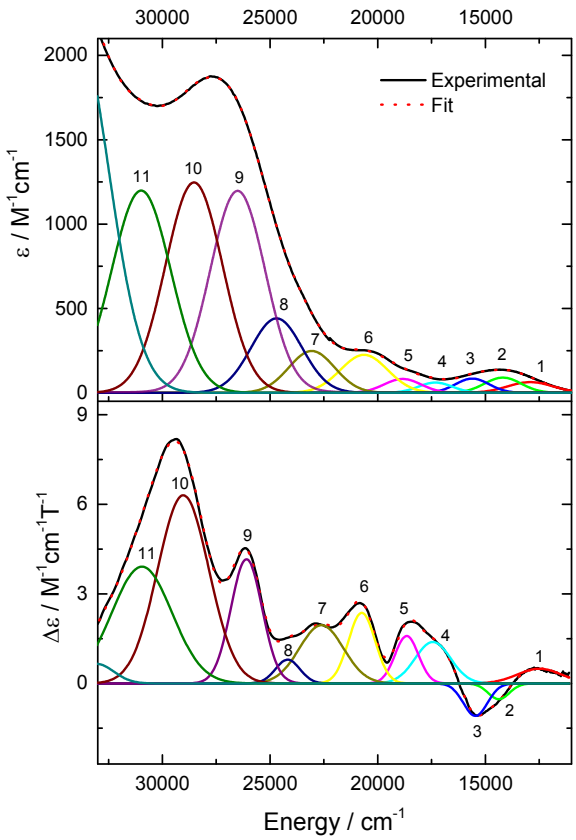

Figure S23. UV-Visible (top, recorded at −70 °C) and MCD (bottom, recorded at 2 K) spectra of the hs-{FeNO}^{8} complex **2**. The colored lines represent a correlated Gaussian deconvolution of the data (see Table S6).

Table S6. Parameters for the correlated fit of the UV-Vis and MCD spectra of complex **2** (see Figure S23).

	UV-Vis			MCD		
Band	**Energy (cm^{-1})**	**ε (M^{-1}cm^{-1})**	**FWHM**	**Energy (cm^{-1})**	**Δε (M^{-1}cm^{-1}T^{-1})**	**FWHM**
1	12910	60	1050	12490	0.5	1030
2	14190	90	850	14380	-0.5	490
3	15610	80	780	15470	-1.1	560
4	17320	60	790	17440	1.4	820
5	18850	80	860	18650	1.6	540
6	20640	230	1090	20740	2.4	620
7	23070	250	1060	22610	1.9	1020
8	24700	440	1190	24180	0.8	570
9	26480	1200	1280	26100	4.2	730
10	28530	1250	1330	29030	6.3	1190
11	30990	1200	1370	30950	3.9	1400

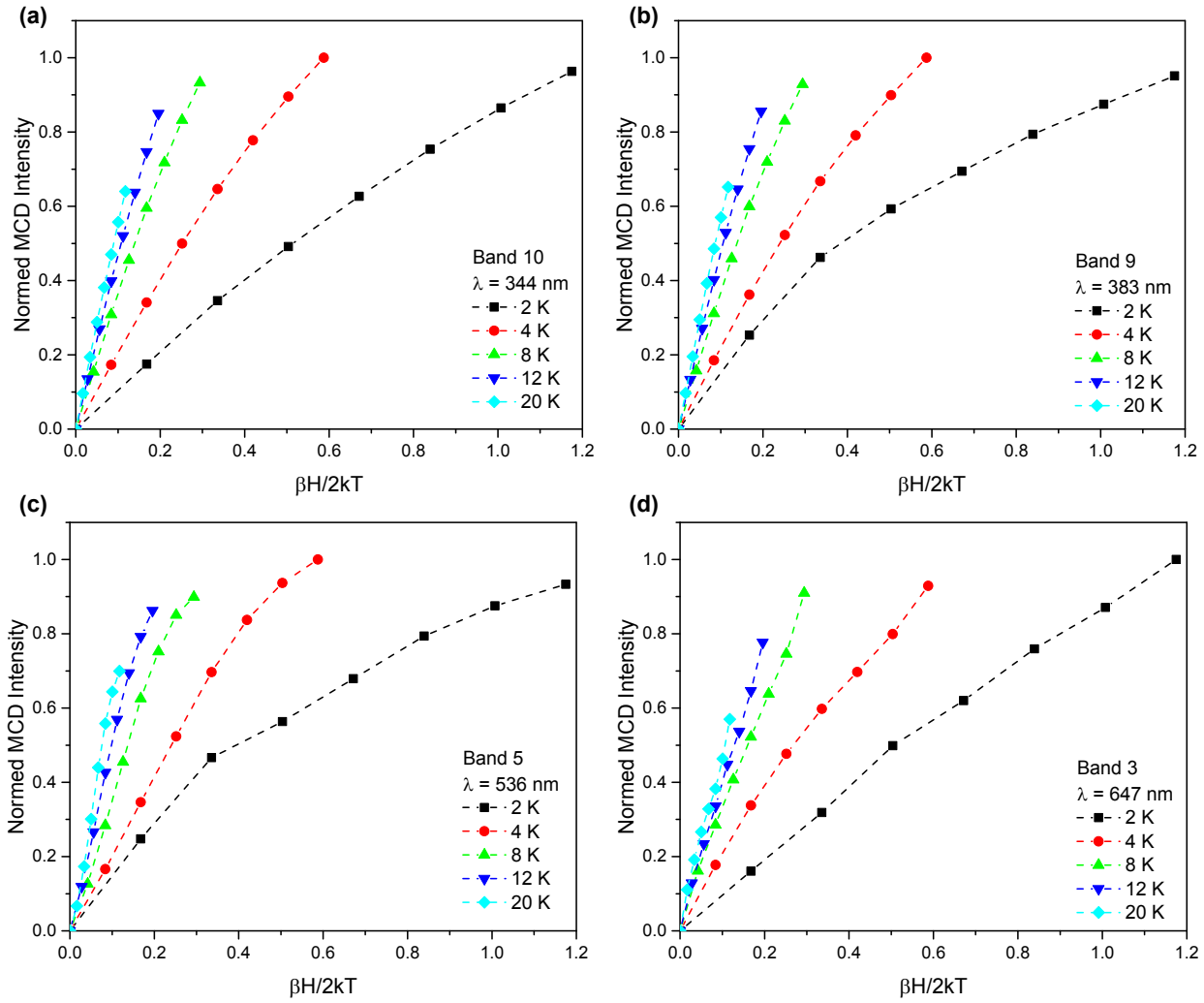

Figure S24. VTVH saturation curves for the MCD features at (a) 344 nm, (b) 383 nm, (c) 536 nm, and (d) 647 nm of complex **2**. Note that overall, the saturation curves for each of these MCD features are very similar. Fitting of these features was therefore not attempted (the lines connecting the data points do ***not*** correspond to a fit, but are just added as a guideline for the eye).

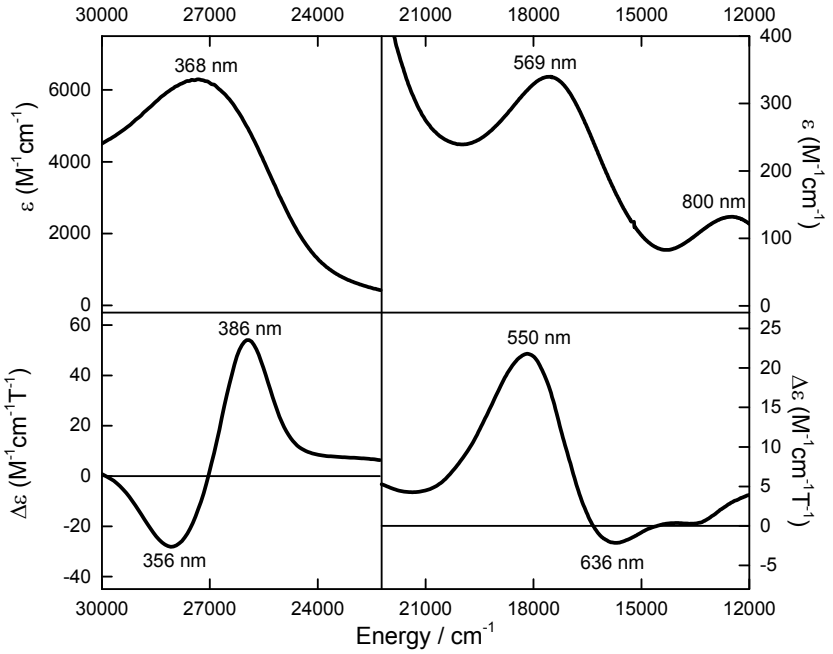

Figure S25. Comparison of the UV-Visible (top, recorded at room temperature) and MCD (bottom, recorded at 2 K) spectra of complex **1**.

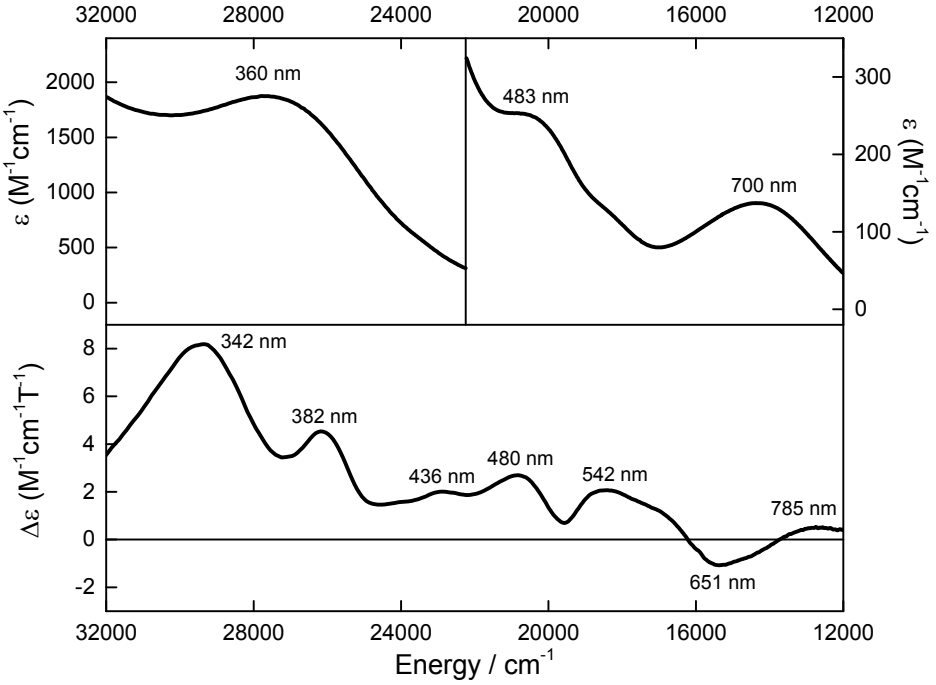

Figure S26. UV-Visible (top, recorded at room temperature) and MCD (bottom, recorded at 2 K) spectra of complex **2**.

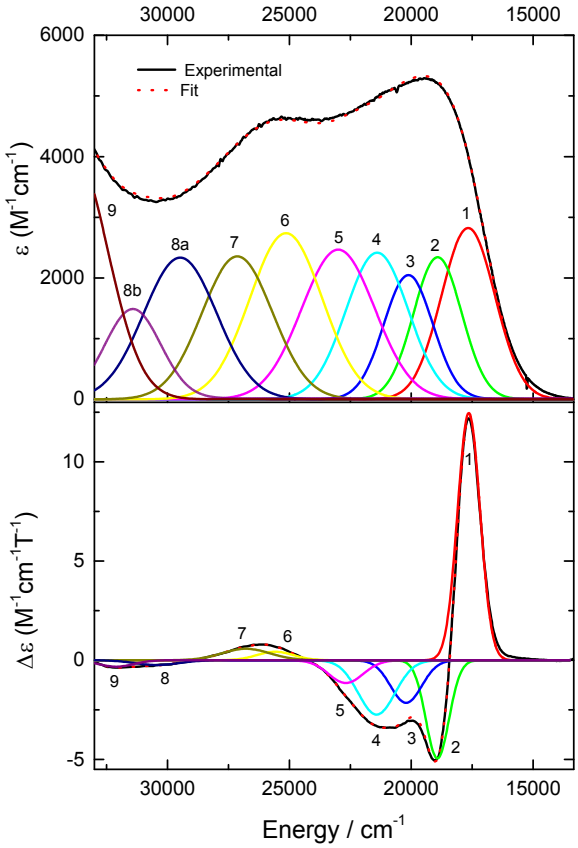

Figure S27. UV-Visible (top, recorded at room temperature) and MCD (bottom, recorded at 50 K) spectra of the hs-{FeNO}^{6} complex **3**. The colored lines represent a correlated Gaussian deconvolution of the data (see Table S7).

Table S7. Parameters for the correlated fit of the UV-Vis and MCD spectra of complex **3** (see Figure S27).

	UV-Vis			MCD		
Band	**Energy (cm^{-1})**	**ε (M^{-1}cm^{-1})**	**FWHM**	**Energy (cm^{-1})**	**Δε (M^{-1}cm^{-1}T^{-1})**	**FWHM**
1	17660	2820	1100	17640	12.5	460
2	18920	2340	990	18930	-4.9	470
3	20120	2050	1000	20210	-2.1	640
4	21400	2420	1280	21420	-2.7	750
5	23000	2470	1500	22680	-1.2	710
6	25140	2740	1490	25580	0.4	750
7	27140	2360	1450	26780	0.6	980
8	29480 31400	2340 1480	1500 1140	30440	-0.2	890
9	33840	4030	1390	32110	-0.3	720

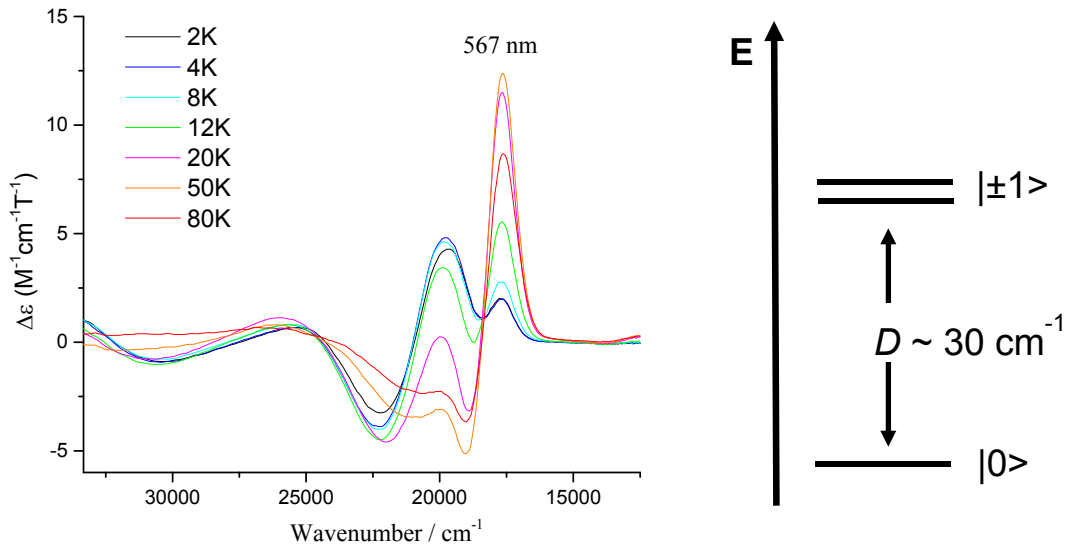

Figure S28. Left: variable temperature MCD spectra for **3** taken at 7 T, showing a significant *increase* in the **C**-term intensity of the bands at 17636 cm^{-1} (567 nm) and 18926 cm^{-1} (528 nm) from 2 K to 50 K. As illustrated on the right, this arises from the Boltzmann *population* of the magnetic $|M_S>$ sublevels of the ground state at higher temperature, caused by very large, positive zero-field splitting (D ~ 30 cm^{-1}, see Figure 11)

SI Figures and Tables Section 2.7

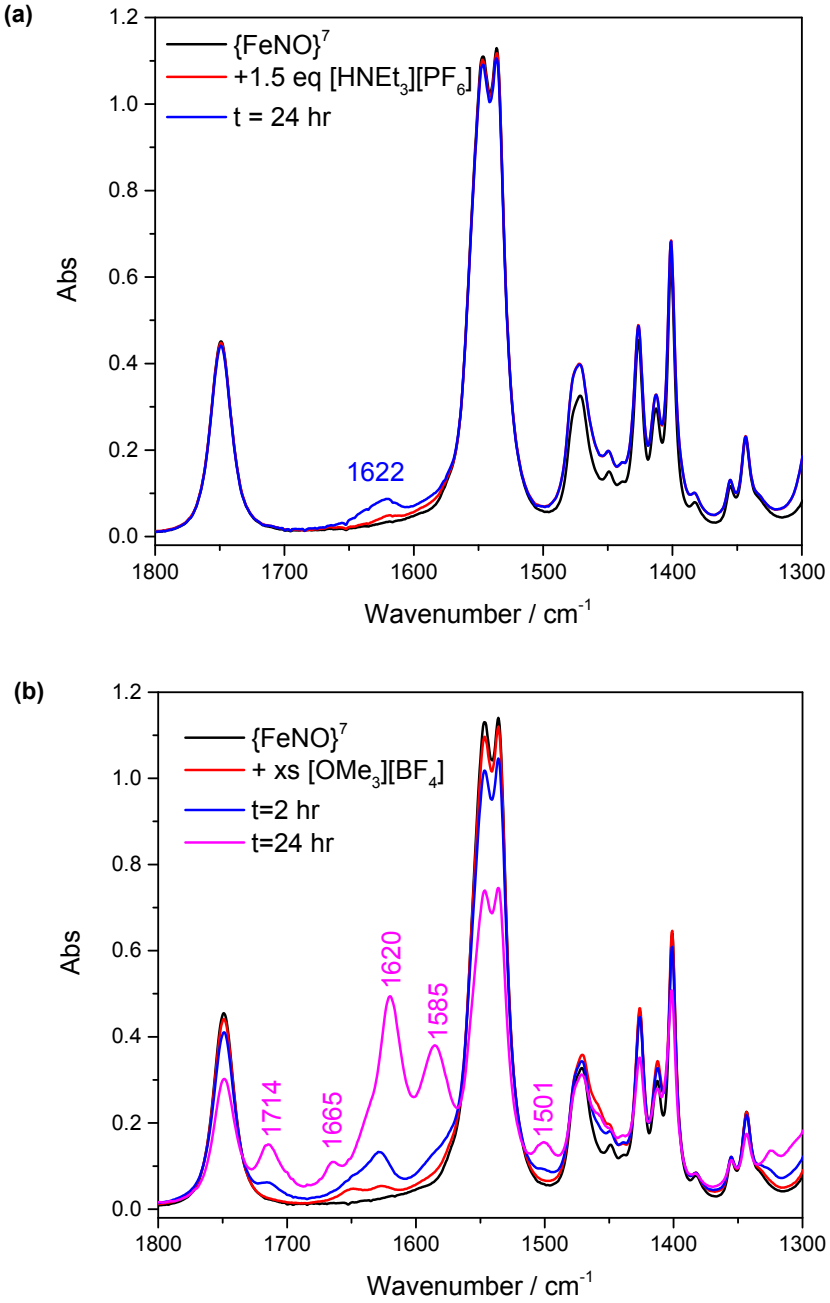

Figure S29. (a) Solution IR data of the hs-{FeNO}^{7} complex **1** before (black line) and after (red line) the addition of the weak acid [$HNEt_3$][PF_6], demonstrating that the complex cannot be protonated by this weak acid, as previously reported.[2] (b) Solution IR spectrum of complex **1** before and after the addition of excess [OMe_3][BF_4], showing that the hs-{FeNO}^{7} complex **1** reacts only slowly with [OMe_3][BF_4]. In contrast, the reaction of the hs-{FeNO}^{8} complex **2** with [OMe_3][BF_4] occurs within mixing time.

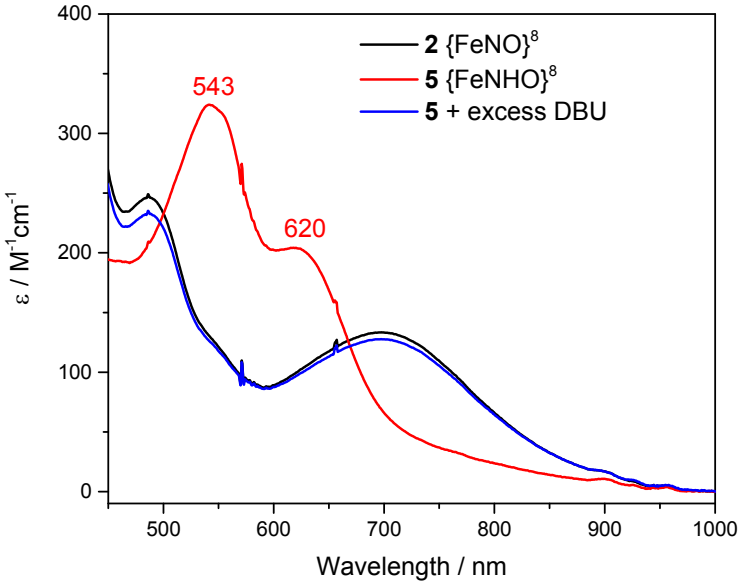

Figure S30. UV-Visible spectra showing the protonation of **2** (black line) to give **5** (red line) at –70°C in 1:1 propionitrile:butyronitrile solution, and deprotonation of **5** (using DBU) after 10 minutes to regenerate **2** (blue line).

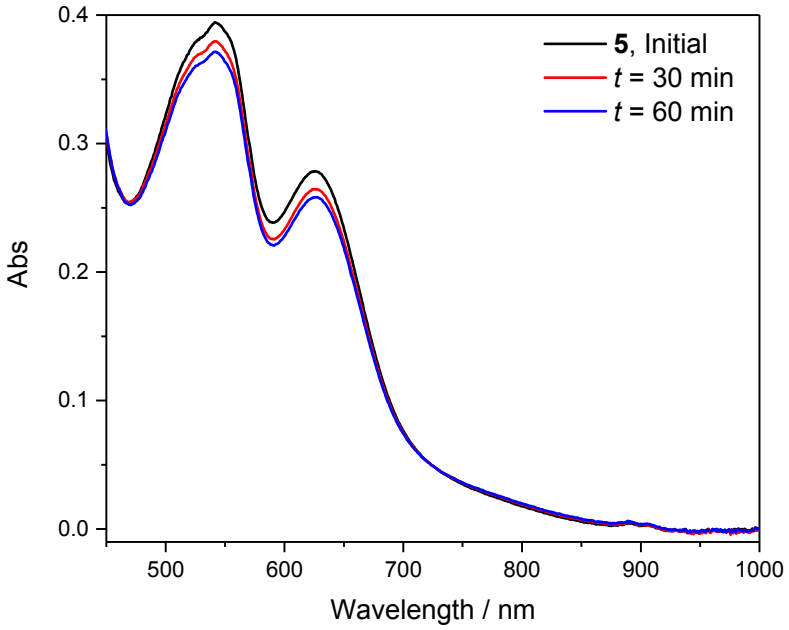

Figure S31. UV-Visible spectrum showing the stability of **5** at –70 °C in acetone.

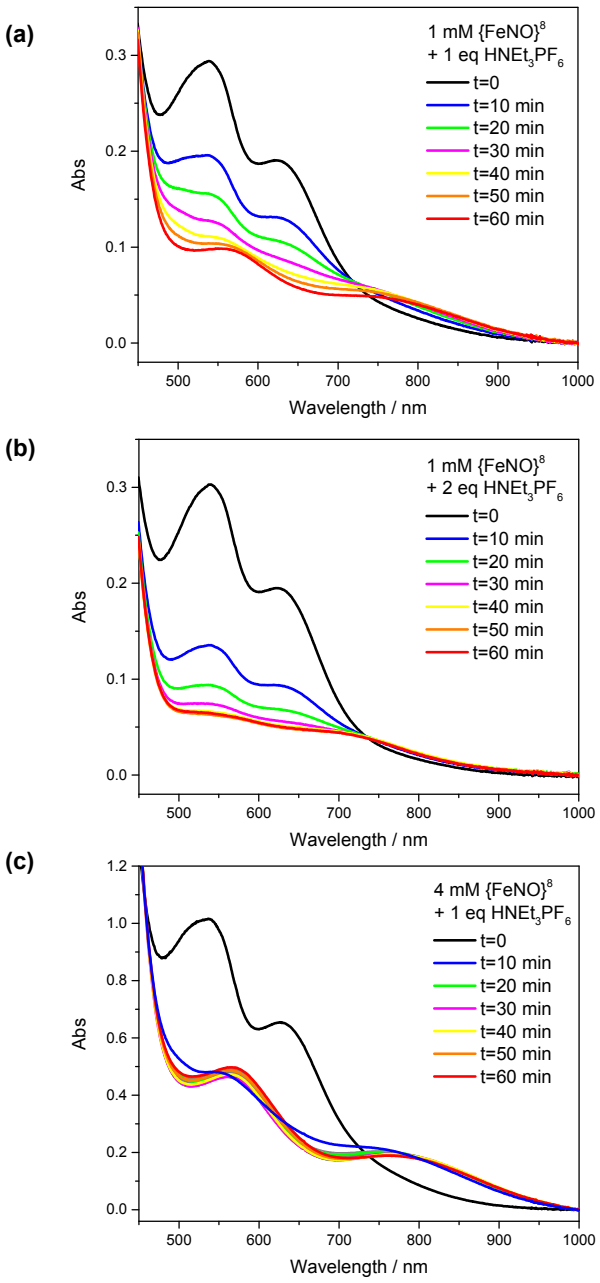

Figure S32. UV-Visible spectra showing the decomposition of **5** at room temperature in CH_3CN (a) at 1 mM in the presence of 1 equivalent of $HNEt_3PF_6$ (b) at 1 mM in the presence of 2 equivalents of $HNEt_3PF_6$, and (c) at 4 mM in the presence of 1 equivalent of $HNEt_3PF_6$. These data show that **5** decomposes more quickly in the presence of excess acid and at higher concentration, and that decomposition under different conditions leads to different product distributions.

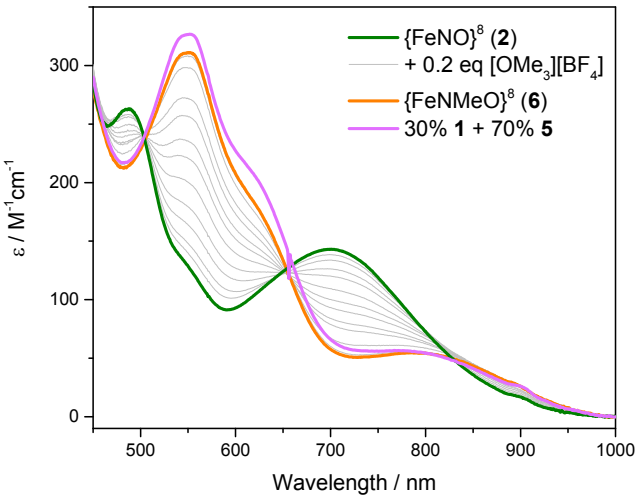

Figure S33. UV-Visible spectra showing the slow addition of 2 equivalents of $[OMe_3][BF_4]$ to **2** (green) at –70°C in 1:1 propionitrile:butyronitrile solution, resulting in partial conversion to complex **6**. The final spectrum (shown in orange) can be modeled with an approximately 30% contribution from **1** and an approximately 70% contribution from a species with UV-Visible features identical to **5** (the combined (predicted) spectrum is shown in purple), which we assign as complex **6**.

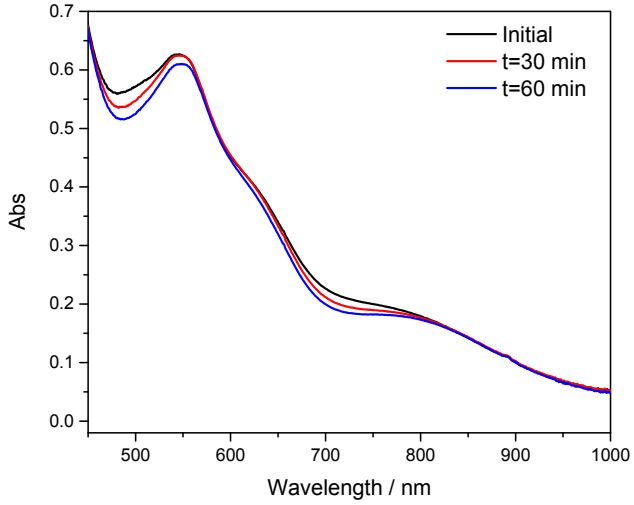

Figure S34. UV-Visible spectrum showing the stability of **6** at –45 °C in CH_3CN.

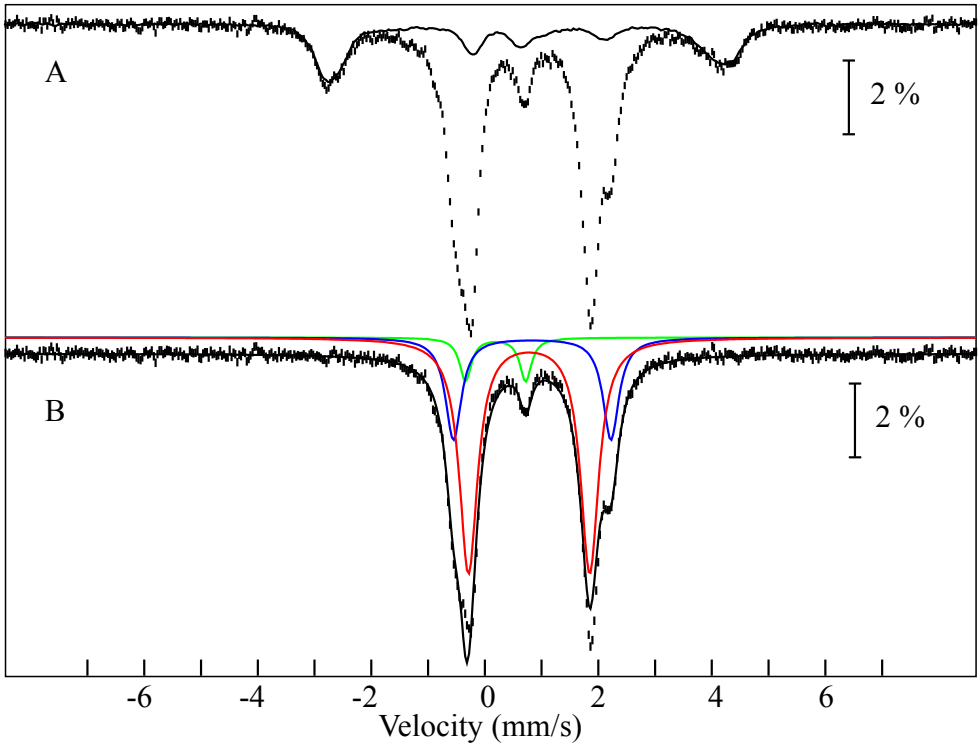

Figure S35. 4.2 K/53 mT Mössbauer characterization of a sample containing complex **6** (5 mM ^{57}Fe-containing species in frozen 1:1 propionitrile:butyronitrile solution). (A) The spectrum of the sample is shown as vertical bars. The overlaying solid line is an experimental spectrum of the hs-{FeNO}^{7} complex recorded under identical conditions, scaled to 25% of total ^{57}Fe absorption. (B) The experimental reference spectrum of **6** after removal of the spectral contributions from hs-{FeNO}^{7} is shown as black vertical bars. The spectrum can be analyzed as superposition of three quadrupole doublets arising from the following species: Me{FeNO}^{8} (δ = 0.78 mm/s, $|\Delta E_Q|$ = 2.14 mm/s, 50%, red line), hs-{FeNO}^{8} (δ = 0.84 mm/s, $|\Delta E_Q|$ = 2.78 mm/s, 19%, blue line), and a small amount of an impurity (tentatively assigned as DNIC based on its Mössbauer parameters of δ = 0.19 mm/s, $|\Delta E_Q|$ = 1.06 mm/s, 6%, green line). The black solid line shows the added contributions of the above species.

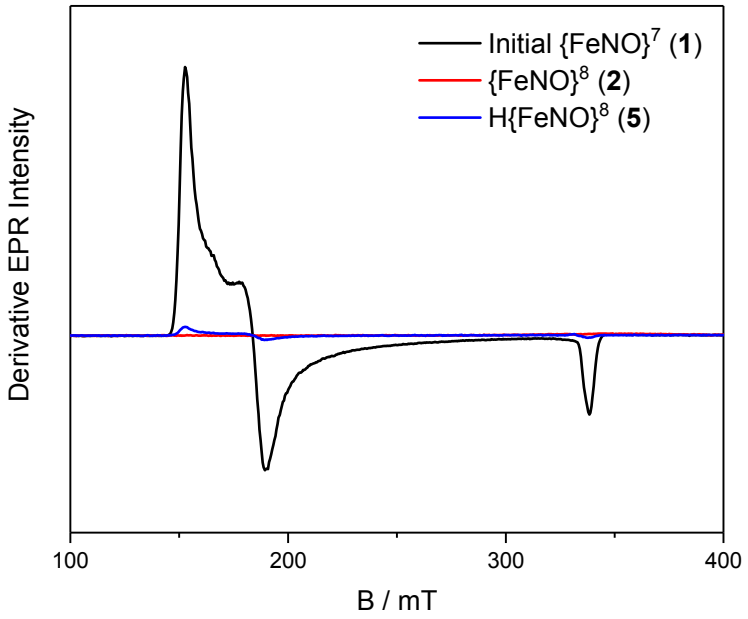

Figure S36. EPR spectra (recorded at 4.2 K) showing the reduction of **1** to **2** and the protonation of **2** to give **5** in 1:1 propionitrile:butyronitrile, demonstrating that **5** contains a negligible amount of **1**. An aliquot of this solution was used to obtain the MCD spectra in Figure S37.

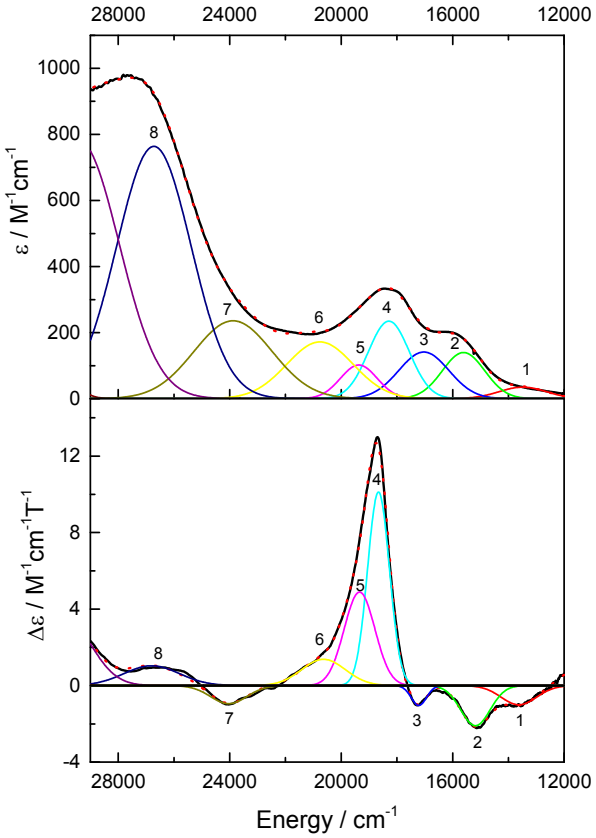

Figure S37. UV-Visible (top, recorded at –70°C) and MCD (bottom, recorded at 4 K) spectra of **5** in 1:1 propionitrile:butyronitrile solution. The solid black line shows the experimental data, and the dashed red line corresponds to the fit. The colored lines represent a correlated Gaussian deconvolution of the data (see Table S8).

Table S8. Parameters for the correlated fit of the UV-Vis and MCD spectra of complex **5** (see Figure S37).

	UV-Vis			MCD		
Band	**Energy (cm^{-1})**	**ε ($M^{-1}cm^{-1}$)**	**FWHM**	**Energy (cm^{-1})**	**Δε ($M^{-1}cm^{-1}T^{-1}$)**	**FWHM**
1	13490	40	850	13630	-1.0	630
2	15610	140	760	15180	-2.1	530
3	17040	140	900	17220	-1.0	270
4	18290	240	740	18660	10.1	390
5	19370	100	660	19340	4.9	550
6	20760	170	1190	20640	1.4	790
7	23880	240	1400	24040	-0.9	650
8	26720	760	1330	26800	1.0	1000

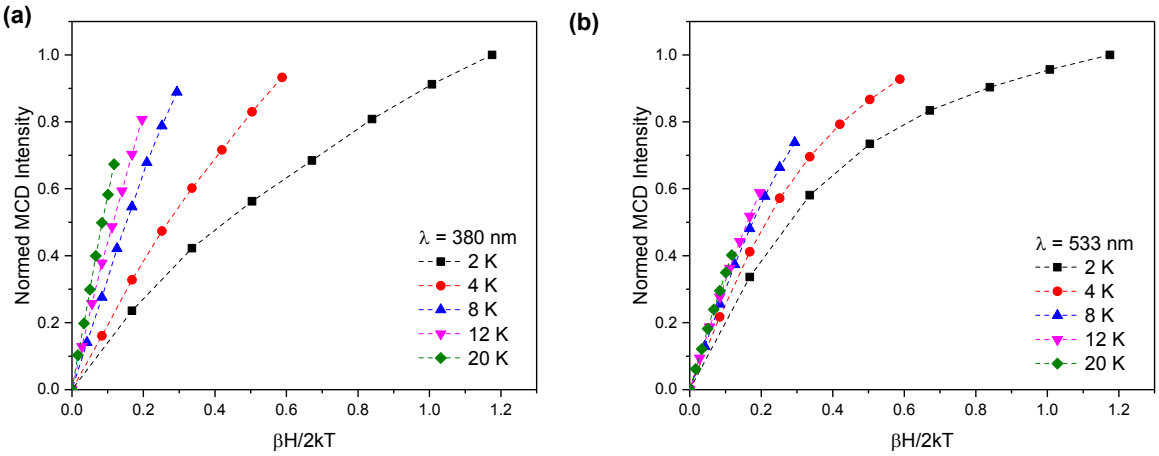

Figure S38. VTVH MCD saturation curves for the bands at (a) 380 nm (band 8) and (b) 533 nm (band 4) of complex **5** (see Table S8). Note that the lines connecting the data points are added as a guideline to the eye and do ***not*** correspond to a fit.

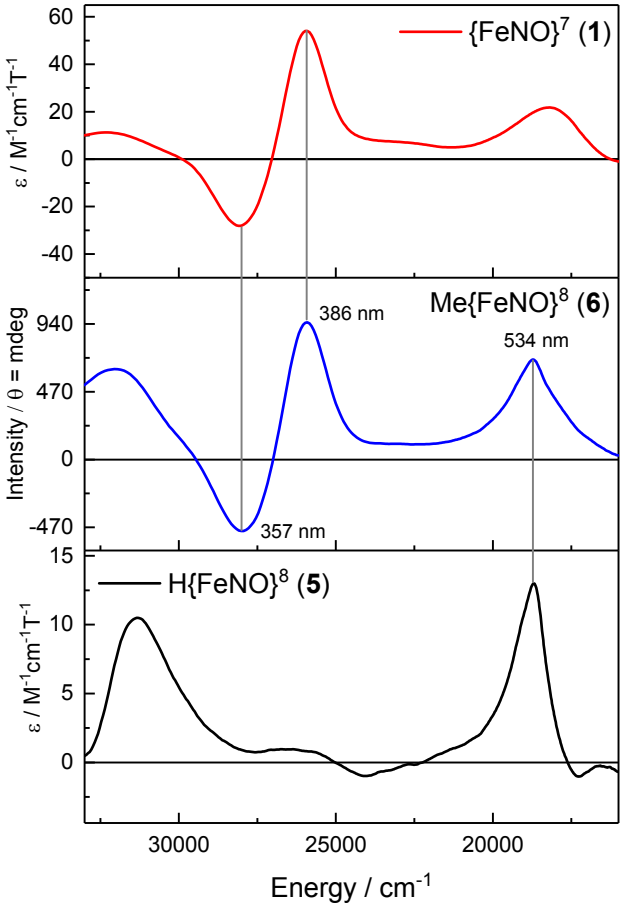

Figure S39. Comparison of the MCD spectrum of complex **6** (middle, blue) at 2 K / 7 T to the spectra of complex **1** (top, red) and complex **5** (bottom, black). The derivative-shaped feature at high energy in the spectrum of **6** arises from a hs-$\{FeNO\}^7$ contaminant. However, the sharp feature at 533 nm, characteristic of the protonated complex **5**, is also present, indicating the presence of the alkylated complex **6**.

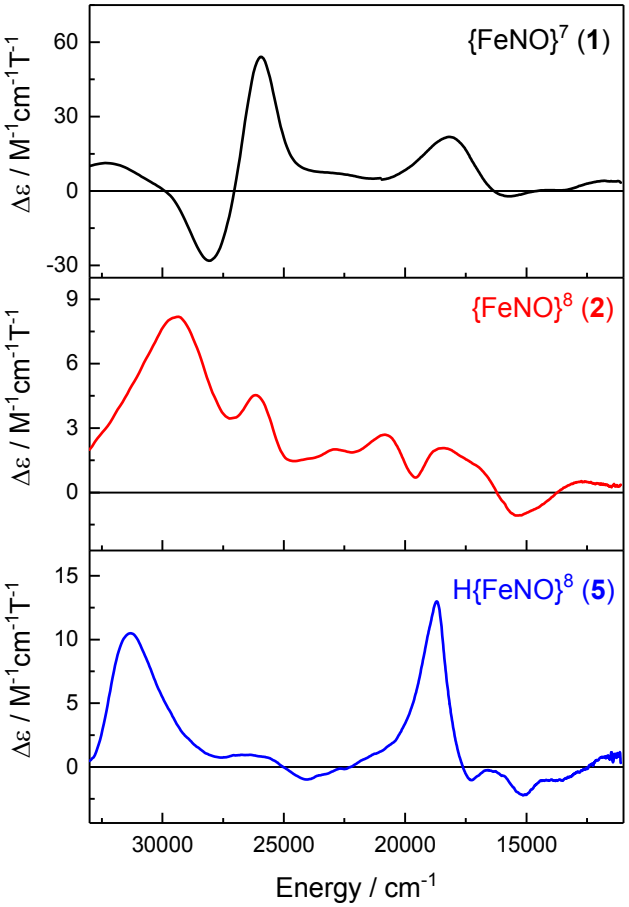

Figure S40. Direct comparison of the MCD data (taken at 2 K) of the hs-{FeNO}^{7} (top), hs-{FeNO}^{8} (middle), and the H{FeNO}^{8} complex (bottom).

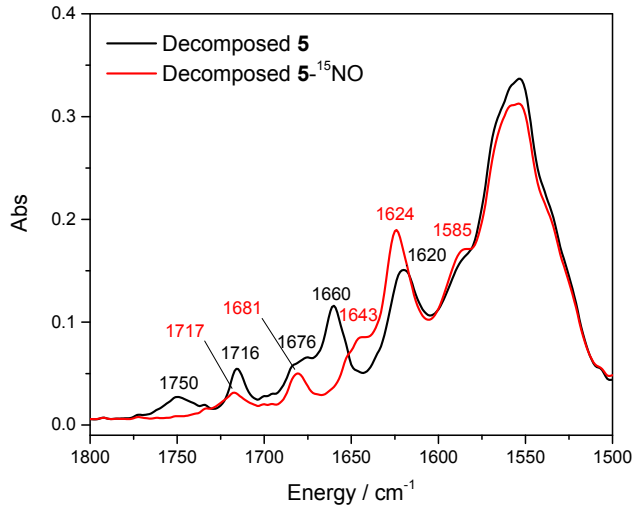

Figure S41. Solution IR spectra of **2** after treatment with 1 equivalent of $[HNEt_3][PF_6]$ at room temperature in propionitrile. The spectrum with natural abundance NO is shown in black, and the corresponding spectrum with ^{15}NO is shown in red.

Decomposition of the H{FeNO}^{8} Complex (5).

In order to gain further information about the fate of complex **5**, the products of its decomposition at room temperature were examined using solution IR spectroscopy (see Figure S41). The IR spectrum reveals multiple isotope-sensitive features between 1750 cm^{-1} and 1550 cm^{-1}. First, a small amount of **1** (ν(N-O) = 1750 cm^{-1}) is formed. The formation of hs-{FeNO}^{7} (likely accompanied by release of H_2) is also observed upon decomposition of heme ls-{FeHNO}^{8} model complexes in the absence of steric protection.[23-26] However, in principle the steric bulk of the TMG_3tren ligand should prevent dimerization and H_2 release; in the case of **5**, the hs-{FeNO}^{7} complex may therefore be formed through a different process. In addition, a prominent feature which is not isotope-sensitive is observed at 1620 cm^{-1}; we assign this feature to a protonated guanidine unit. (The spectrum of independently prepared free $H_3TMG_3tren^{3+}$ in solution exhibits bands at 1620 cm^{-1} and 1584 cm^{-1}).[21] The finding of ligand protonation is not surprising, given the high proton affinity of guanidine ligands. Accordingly, it has been demonstrated in the literature that upon exposure to water, metal TMG_3tren complexes decompose into metal hydroxide complexes and protonated ligand.[21]

Our spectroscopic data and DFT results indicate that addition of a weak acid to **2** generates a ligand protonated species, H{FeNO}^{8}, which we identify with **5**. Dissociation of the protonated guanidine moiety results in a hs-{FeNO}^{8} complex with an open coordination site which, as discussed in Section 2.2 in the paper, is unstable and decays to produce an {Fe(NO)$_2$}^{10} DNIC and a ferrous species. This is directly demonstrated for the less-hindered complex [Fe(TMG_2dien)(NO)(OTf)](OTf) (**4**) in which one of the guanidine arms has been removed: upon reduction, this complex immediately forms an {Fe(NO)$_2$}^{10} DNIC (and a ferrous species). In the spectrum shown in Figure S41, it is unclear whether the expected DNIC species with ν(NO) = 1672, 1614 cm^{-1} (*c.f.* Figure 2) is present in solution. However, two additional isotope-

sensitive features are observed at 1716 cm^{-1} and 1660 cm^{-1}. Based on their energies, the separation between them, and the ratio of their intensities, these could potentially correspond to an $\{Fe(NO)_2\}^{10}$ DNIC with a different coordination environment compared to the one resulting from the reduction of the hs-$\{FeNO\}^7$ TMG_2dien complex. In addition, a number of other products are also formed in the decomposition of **5**, as mentioned above.

Table S9. Key structural parameters for DFT-optimized structures of **2** and of N-, O-, and ligand-protonated versions of complex **5**. The N- and O-protonated complexes were optimized in the gas-phase and the CPCM solvent model (acetonitrile) was used for the optimization of the 4c and 5c ligand-protonated species.

	{FeNO}^{8} *S* = 1[3]	**HNO S = 2**	**HNO S = 1**	**NOH S = 2**	**NOH S = 1**	**4C lig-prot** [b] **S = 1**	**5C lig-prot** [c] **S = 1**
Fe-N(O)	1.694	1.960	1.792	1.743	1.728	1.661	1.694
N-O	1.202	1.251	1.249	1.346	1.380	1.205	1.205
Fe-N-O	159	131	133	137	119	167	151
H-N-O / N-O-H	-	111	113	104	105	-	-
Fe-N(amine)	2.360	2.279	2.089	2.153	2.146	2.165	2.534/1.974[d]
Avg. Fe-N(guan)	2.160	2.093	2.049	2.072	2.050	2.026	2.083
Energy difference[a]	-	+22.9	+8.7	+33.2	+25.5	0	+4.7

[a] Calculated at the TPSS/def2-TZVP(-f) level. [b] Four-coordinate, ligand-protonated structure. [c] Five-coordinate, ligand protonated structure with an acetonitrile solvent molecule coordinated to the iron center. [d] Fe-NCMe distance

Table S10. Key structural parameters for DFT-optimized structures of N- and O-methylated versions of complex (**6**).

	CH_3NO *S* = 2	**CH_3NO *S* = 1**	**$NOCH_3$ *S* = 2**	**$NOCH_3$ *S* = 1**
Fe-N	2.003	1.833	1.754	1.739
N-O	1.250	1.249	1.334	1.352
Fe-N-O	121	124	141	120
CH_3-N-O / N-O-CH_3	113	112	114	112
Fe-N(amine)	2.313	2.116	2.193	2.153
Avg. Fe-N(guan)	2.112	2.087	2.083	2.058
Energy difference[a]	+8.6	0.0	+20.7	+11.7

[a] Calculated at the TPSS/def2-TZVP(-f) level

Table S11. Comparison of experimental and DFT-calculated Mössbauer parameters for TMG_3tren complexes.

Compound	**Expt. δ (mm/s)**	**DFT δ (mm/s)**	**Expt. ΔE_Q (mm/s)**[a]	**DFT ΔE_Q (mm/s)**	**Ref.**
{FeNO}^{6} (**3**)	0.06	0.07	0.48	+0.40	3
{FeNO}^{7} (**1**)	0.48	0.38	–1.42	–1.69	3
{FeNO}^{8} (**2**)	0.84	0.72	–2.78	+2.13	3
Fe(II)-CH_3CN	0.98	0.84	1.64	+3.41	*t.w.*
Fe(IV)=O	0.09	0.07	–0.29	–0.55	22,27
Fe(IV)-CN	–0.19	–0.21	–4.45	–5.25	28
H{FeNO}^{8} (**5**)	0.78	-	2.14	-	*t.w.*
{FeHNO}^{8}, *S* = 2	-	0.48	-	+2.11	
{FeHNO}^{8}, *S* = 1	-	0.33	-	+2.13	
{FeNOH}^{8}, *S* = 2	-	0.37	-	+1.60	
{FeNOH}^{8}, *S* = 1	-	0.25	-	+2.80	
4C H{FeNO}^{8}, *S* = 1	-	0.44	-	+1.70	
5C H{FeNO}^{8}, *S* = 1	-	**0.63**	-	+1.73	
CH_3 {FeNO}^{8} (**6**)	0.78	-	2.14	-	*t.w.*
{FeCH_3NO}^{8}, *S* = 2	-	0.57	-	+2.34	
{FeCH_3NO}^{8}, *S* = 1	-	0.42	-	+2.00	
{Fe$NOCH_3$}^{8}, *S* = 2	-	0.37	-	–2.00	
{Fe$NOCH_3$}^{8}, *S* = 1	-	0.30	-	+2.84	

[a] Unless specified, the sign of ΔE_Q was not determined.

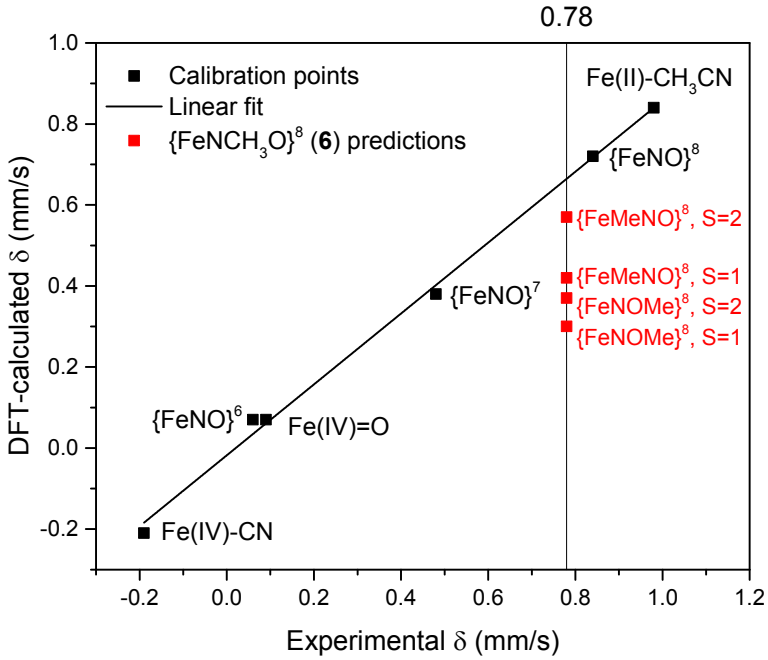

Figure S42. Correlation of experimental and DFT-calculated Mössbauer isomer shifts for TMG_3tren complexes (black squares). The DFT-predicted values for the different possible identities of **6** are plotted as red squares at the experimentally observed value of $\delta = 0.78$ mm/s.

Table S12. DFT-optimized coordinates of $[Fe(TMG_3tren)(O)]^{2+}$ ($S = 2$)

Fe	2.524660	4.420427	6.365301
O	3.816273	4.484143	5.342487
N	0.872783	4.343283	7.674142
N	3.417316	3.362952	7.851701
N	1.248559	3.444833	5.120174
N	2.288095	6.423357	6.609594
N	5.403724	2.861581	9.060289
N	5.204017	2.220289	6.837151
N	0.945490	1.849552	3.381866
N	2.044996	3.847869	2.944948
N	2.447720	8.602461	5.669118
N	4.374388	7.378684	6.097989
C	1.153329	3.288523	8.701975
H	0.941649	2.317832	8.248019
H	0.490783	3.419901	9.566689
C	2.619003	3.360693	9.098673
H	2.798265	4.259510	9.701616
H	2.875410	2.498244	9.723661
C	4.662233	2.839253	7.913174
C	5.389759	3.989915	9.998686
H	4.894670	4.844923	9.541550
H	6.424470	4.265316	10.227776
H	4.886914	3.727128	10.936181
C	6.286802	1.747858	9.448873
H	6.079272	0.879338	8.824919
H	6.078448	1.493961	10.493047
H	7.343909	2.020729	9.361526
C	6.642398	2.271225	6.539474
H	7.135217	2.973108	7.210823
H	6.766016	2.618399	5.508678
H	7.106115	1.283863	6.635811
C	4.391016	1.532769	5.833272
H	3.374996	1.434669	6.212346
H	4.818946	0.538891	5.660656
H	4.377341	2.096653	4.896770
C	-0.338633	3.997988	6.861131
H	-0.674014	4.909546	6.361538
H	-1.143981	3.644627	7.517267
C	0.041616	2.954198	5.823605
H	0.217088	1.988476	6.313676
H	-0.787428	2.812074	5.121712
C	1.423953	3.044074	3.840989
C	0.937985	0.626747	4.193421
H	1.546437	0.770614	5.084588
H	1.370266	-0.186790	3.601585
H	-0.080057	0.341092	4.481101
C	0.398011	1.690632	2.023125
H	0.244767	2.670136	1.571706
H	-0.566842	1.179433	2.100257

H	1.059399	1.091290	1.388382
C	2.885417	3.319231	1.861237
H	3.029461	2.247708	1.992919
H	3.858858	3.817659	1.909468
H	2.440298	3.511719	0.879404
C	2.006862	5.307677	3.038891
H	1.260359	5.591721	3.778855
H	1.729088	5.711972	2.059013
H	2.982590	5.700030	3.337374
C	0.729821	5.693521	8.310029
H	1.467219	5.762160	9.112915
H	-0.271049	5.799634	8.746982
C	1.005961	6.764101	7.266814
H	0.176685	6.809015	6.550089
H	1.065264	7.745060	7.750983
C	3.021789	7.446518	6.116791
C	1.169800	8.632616	4.948160
H	0.887458	7.623389	4.653643
H	1.293278	9.239633	4.045243
H	0.375046	9.077759	5.557269
C	3.071756	9.921769	5.872152
H	3.888438	9.835790	6.587922
H	2.314009	10.600377	6.276460
H	3.447433	10.340190	4.932269
C	5.180471	7.993822	5.033992
H	4.530075	8.359285	4.240458
H	5.846440	7.227993	4.623689
H	5.788711	8.818944	5.419140
C	5.136451	6.606697	7.080222
H	4.469077	6.312399	7.888735
H	5.938064	7.241096	7.474756
H	5.565581	5.713298	6.618894

Table S13. DFT-optimized coordinates of $S = 2$ $\{FeHNO\}^8$ complex

Fe	0.000994	0.012100	0.253196
N	-0.224593	-0.180208	-1.684644
N	-0.059846	-0.024265	2.530761
N	-2.053461	-0.368411	0.600646
N	0.705303	1.919245	0.644825
N	1.307660	-1.573761	0.645841
N	-4.167290	-1.184912	-0.140829
N	-3.153936	0.612733	-1.225196
N	1.034488	4.179423	-0.037938
N	2.184256	2.461573	-1.096731
N	3.131133	-2.937548	-0.058982
N	1.088523	-3.054030	-1.165766
C	-1.487312	-0.029197	2.945045
H	-1.850519	1.001593	2.919559
H	-1.596915	-0.403152	3.972401
C	-2.299923	-0.872740	1.969294
H	-2.012876	-1.928240	2.063589
H	-3.361873	-0.801845	2.227123
C	-3.107700	-0.326921	-0.232106
C	-4.018176	-2.588724	0.261752
H	-2.965693	-2.866392	0.243063
H	-4.561873	-3.215370	-0.452953
H	-4.428431	-2.768946	1.261523
C	-5.555996	-0.757159	-0.386522
H	-5.600781	0.328312	-0.465299
H	-6.168181	-1.073116	0.464237
H	-5.963143	-1.211497	-1.296009
C	-3.831883	0.381365	-2.509681
H	-4.039900	-0.681291	-2.632054
H	-3.167987	0.712110	-3.315348
H	-4.767641	0.946185	-2.582648
C	-2.628278	1.967690	-1.039102
H	-2.241404	2.055780	-0.024979
H	-3.437641	2.691516	-1.193004
H	-1.828646	2.178475	-1.756494
C	0.642037	1.210065	2.980435
H	1.716132	1.007570	2.980949
H	0.345927	1.474806	4.004828
C	0.345901	2.351792	2.015120
H	-0.714813	2.627939	2.082517
H	0.927506	3.232234	2.308004
C	1.283057	2.840760	-0.154735
C	-0.282276	4.717726	0.319814
H	-1.025789	3.924005	0.287913
H	-0.557102	5.487431	-0.409215
H	-0.272635	5.172971	1.316444
C	2.076119	5.197316	-0.259315
H	3.054121	4.719645	-0.302486
H	2.058065	5.894288	0.584676

H	1.901031	5.762405	-1.181024
C	2.312350	3.141300	-2.394788
H	1.501296	3.857708	-2.517516
H	2.240523	2.386426	-3.183198
H	3.274687	3.656753	-2.480992
C	3.028832	1.280060	-0.932603
C	0.650913	-1.254802	2.970645
H	-0.055298	-2.088086	2.924014
H	0.994235	-1.158220	4.009954
C	1.821026	-1.532999	2.033077
H	2.585596	-0.754476	2.155338
H	2.284881	-2.486391	2.308207
C	1.845134	-2.495860	-0.174271
C	4.235507	-2.076744	0.380571
H	3.912896	-1.038065	0.384846
H	5.065300	-2.186519	-0.325372
H	4.590028	-2.357723	1.378336
C	3.517236	-4.331650	-0.339326
H	2.626263	-4.950255	-0.437352
H	4.110662	-4.698201	0.504233
H	4.122111	-4.407013	-1.249132
C	1.650631	-3.446465	-2.465615
H	2.654570	-3.037164	-2.569994
H	1.017969	-3.030447	-3.256857
H	1.683775	-4.535263	-2.583024
C	-0.317770	-3.397894	-0.964505
H	-0.623888	-3.073305	0.028955
H	-0.447719	-4.483487	-1.056499
H	-0.951225	-2.919767	-1.721042
O	0.452973	0.273894	-2.633778
H	2.700630	0.473864	-1.596908
H	2.978629	0.954163	0.106037
H	4.061104	1.549233	-1.182711
H	-1.028419	-0.749203	-2.039179

Table S14. DFT-optimized coordinates for $S = 1$ $\{FeHNO\}^8$ complex

Fe	-0.020613	-0.002980	0.392183
N	0.077771	-0.064251	-1.396477
N	-0.018932	-0.030990	2.480821
N	1.221818	-1.651838	0.624245
N	-2.026632	-0.269435	0.643609
N	0.791009	1.838666	0.646760
N	2.986477	-3.082448	-0.106140
N	0.982540	-2.950477	-1.310313
N	-4.107344	-1.104377	-0.157558
N	-3.130858	0.754345	-1.157097
N	1.165371	4.066521	-0.097745
N	2.194525	2.295077	-1.188398
C	0.592253	-1.319618	2.938289
H	-0.178749	-2.092379	2.889414
H	0.927179	-1.231582	3.979653
C	1.738700	-1.685019	2.011358
H	2.567770	-0.979135	2.148077
H	2.115157	-2.680932	2.269360
C	1.738646	-2.544764	-0.230133
C	4.138453	-2.325671	0.401302
H	3.908364	-1.262001	0.406040
H	4.986056	-2.498655	-0.269725
H	4.423737	-2.647245	1.408923
C	3.269729	-4.496145	-0.414419
H	2.337735	-5.039396	-0.564661
H	3.793457	-4.934363	0.441063
H	3.905054	-4.595635	-1.300634
C	1.587994	-3.396649	-2.576959
H	2.608099	-3.020190	-2.649821
H	0.997825	-2.988133	-3.403649
H	1.593070	-4.488260	-2.668195
C	-0.441490	-3.278350	-1.155898
H	-0.757293	-2.988151	-0.155543
H	-0.589945	-4.355681	-1.298695
H	-1.043826	-2.744141	-1.898477
C	-1.437084	0.072612	2.954873
H	-1.726235	1.125413	2.918489
H	-1.513050	-0.274218	3.993319
C	-2.322499	-0.731477	2.018784
H	-2.125833	-1.804515	2.143706
H	-3.375527	-0.565693	2.270828
C	-3.065006	-0.223716	-0.217509
C	-3.947684	-2.504600	0.246571
H	-2.890413	-2.759217	0.279109
H	-4.443995	-3.143313	-0.491755
H	-4.401294	-2.692869	1.226223
C	-5.493659	-0.707816	-0.460199
H	-5.562245	0.377613	-0.518189
H	-6.137060	-1.061363	0.351766

H	-5.843548	-1.149793	-1.399162
C	-3.705178	0.539665	-2.492315
H	-3.887181	-0.523163	-2.648938
H	-2.982975	0.890398	-3.236076
H	-4.641149	1.093902	-2.621856
C	-2.661360	2.116992	-0.891724
C	0.785189	1.141297	2.958509
H	1.840878	0.861665	2.923532
H	0.523545	1.378546	3.997504
C	0.538312	2.314906	2.026168
H	-0.489324	2.680786	2.147915
H	1.209058	3.140532	2.287491
C	1.356987	2.718250	-0.203863
C	-0.107404	4.660824	0.324834
H	-0.883998	3.899365	0.330670
H	-0.384106	5.440839	-0.392226
H	-0.027390	5.117124	1.317961
C	2.231186	5.040503	-0.389598
H	3.186764	4.525744	-0.481401
H	2.287519	5.747453	0.444343
H	2.025271	5.601477	-1.307453
C	2.264462	2.949266	-2.503259
H	1.467243	3.685490	-2.590281
H	2.122391	2.187383	-3.276294
H	3.234285	3.434300	-2.657251
C	3.044405	1.119422	-1.034867
H	2.980455	0.768693	-0.005853
H	4.079398	1.393484	-1.271109
H	2.738231	0.316810	-1.716026
O	-0.240459	0.739742	-2.297269
H	-1.803277	2.358003	-1.523162
H	-2.381585	2.190275	0.158704
H	-3.479060	2.816337	-1.102614
H	0.506302	-0.940938	-1.773234

Table S15. DFT-optimized coordinates of $S = 2$ $\{FeNOH\}^8$ complex

Fe	-0.075013	-0.100284	0.351101
N	-0.057529	-0.068054	-1.391749
N	-0.053259	-0.073007	2.504016
N	1.101229	-1.783225	0.667598
N	-2.090802	-0.152599	0.659548
N	0.868919	1.758744	0.605762
N	2.825332	-3.252593	-0.075770
N	0.826339	-3.105590	-1.250708
N	-4.207797	-0.884718	-0.141390
N	-3.149396	0.932771	-1.132630
N	1.505533	3.956090	-0.038279
N	2.166760	2.105363	-1.330093
C	0.460548	-1.398327	2.972018
H	-0.366344	-2.110719	2.919624
H	0.790213	-1.329690	4.017042
C	1.587167	-1.861452	2.060605
H	2.474106	-1.234215	2.220730
H	1.869775	-2.886714	2.324803
C	1.585977	-2.686245	-0.203937
C	3.988931	-2.521229	0.435788
H	3.769426	-1.455561	0.473006
H	4.830991	-2.682445	-0.245738
H	4.280537	-2.870958	1.432666
C	3.088674	-4.658307	-0.427773
H	2.145992	-5.179342	-0.590511
H	3.614833	-5.130120	0.408365
H	3.714298	-4.740942	-1.323218
C	1.400256	-3.442897	-2.559779
H	2.452982	-3.163860	-2.584778
H	0.863656	-2.877194	-3.328732
H	1.300508	-4.511399	-2.779702
C	-0.631272	-3.198839	-1.170208
H	-0.931611	-3.064166	-0.131745
H	-0.939644	-4.191914	-1.516873
H	-1.107924	-2.433168	-1.789271
C	-1.457045	0.143333	2.973446
H	-1.665407	1.215270	2.935038
H	-1.567283	-0.193160	4.012601
C	-2.405590	-0.591918	2.038951
H	-2.286297	-1.676297	2.162235
H	-3.441811	-0.350298	2.299916
C	-3.128489	-0.052854	-0.197963
C	-4.104025	-2.292169	0.259083

H	-3.058047	-2.590989	0.275824
H	-4.636592	-2.905346	-0.475238
H	-4.554281	-2.462191	1.243523
C	-5.575017	-0.432219	-0.451606
H	-5.599678	0.655276	-0.506953
H	-6.236381	-0.761935	0.355800
H	-5.936442	-0.858091	-1.393587
C	-3.734449	0.751054	-2.468101
H	-3.962508	-0.301912	-2.628881
H	-2.996733	1.070840	-3.210468
H	-4.644471	1.347602	-2.594957
C	-2.612875	2.267424	-0.862173
C	0.845061	1.038256	2.933159
H	1.875737	0.679634	2.875304
H	0.638360	1.321273	3.973861
C	0.667574	2.225105	1.998265
H	-0.332628	2.656800	2.128123
H	1.393624	3.001459	2.261057
C	1.500959	2.602246	-0.216639
C	0.327766	4.693351	0.440988
H	-0.556217	4.062628	0.361731
H	0.192272	5.571450	-0.198739
H	0.450056	5.034217	1.474925
C	2.720417	4.776660	-0.200811
H	3.590814	4.136360	-0.337139
H	2.862972	5.359613	0.714887
H	2.629904	5.468706	-1.044255
C	2.505844	2.963546	-2.485844
H	1.788886	3.780807	-2.562857
H	2.449493	2.350725	-3.391198
H	3.520602	3.369270	-2.417872
C	3.008538	0.899134	-1.215793
H	2.720922	0.356034	-0.318591
H	4.066145	1.188142	-1.169407
H	2.854935	0.256184	-2.086520
O	-0.201225	0.848982	-2.366382
H	-1.777162	2.488943	-1.531015
H	-2.280314	2.310073	0.174093
H	-3.404671	3.008213	-1.025880
H	0.619686	1.410115	-2.299438

Table S16. DFT-optimized coordinates of $S = 1$ $\{FeNOH\}^8$ complex

Fe	-0.002532	-0.030414	0.318782
N	0.185026	-0.117887	-1.396466
N	0.005165	-0.074549	2.464616
N	1.544852	-1.384154	0.607750
N	-1.928482	-0.674228	0.608949
N	0.375703	1.933131	0.616207
N	3.558443	-2.436473	-0.125673
N	1.567976	-2.821370	-1.250502
N	-3.823125	-1.888051	-0.168009
N	-3.307120	0.181570	-1.090564
N	0.392943	4.206502	-0.078888
N	1.776347	2.668639	-1.130362
C	0.903990	-1.176758	2.927834
H	0.333256	-2.108313	2.900391
H	1.224309	-0.998664	3.962586
C	2.085068	-1.279492	1.979960
H	2.730184	-0.397694	2.094516
H	2.689164	-2.156188	2.237562
C	2.218342	-2.177550	-0.243836
C	4.535357	-1.435626	0.314828
H	4.069748	-0.453268	0.347111
H	5.361085	-1.409509	-0.404523
H	4.945123	-1.680881	1.301183
C	4.131836	-3.759549	-0.424961
H	3.332239	-4.491631	-0.532245
H	4.773130	-4.053800	0.412221
H	4.738939	-3.741632	-1.336776
C	2.182145	-3.059513	-2.562052
H	3.141956	-2.548016	-2.619741
H	1.518799	-2.656958	-3.335370
H	2.325959	-4.129079	-2.749511
C	0.171234	-3.225691	-1.136051
H	-0.128832	-3.146285	-0.091786
H	0.075715	-4.265008	-1.470597
H	-0.475901	-2.590056	-1.750060
C	-1.394918	-0.313900	2.931681
H	-1.923886	0.642131	2.929978
H	-1.392110	-0.706942	3.956489
C	-2.066795	-1.266477	1.959743
H	-1.597321	-2.257163	2.019919
H	-3.121920	-1.389037	2.225801
C	-2.989039	-0.807296	-0.211523
C	-3.358238	-3.244290	0.141005

H	-2.271516	-3.272905	0.115539
H	-3.749922	-3.931059	-0.616704
H	-3.713831	-3.574464	1.123515
C	-5.277260	-1.771317	-0.375113
H	-5.570291	-0.722457	-0.355920
H	-5.783188	-2.295216	0.442073
H	-5.587080	-2.224147	-1.322933
C	-3.913748	-0.086390	-2.399736
H	-3.853998	-1.151184	-2.623193
H	-3.354156	0.469414	-3.159202
H	-4.959875	0.237170	-2.437546
C	-3.147371	1.597425	-0.754824
C	0.500076	1.256069	2.934336
H	1.592549	1.240107	2.906246
H	0.183554	1.437769	3.969684
C	-0.015582	2.328478	1.989029
H	-1.105253	2.421736	2.082403
H	0.419621	3.296436	2.257966
C	0.825679	2.915112	-0.191013
C	-0.984742	4.557217	0.282984
H	-1.609110	3.667311	0.250128
H	-1.364073	5.283739	-0.443455
H	-1.034652	5.008144	1.280456
C	1.289191	5.358663	-0.277883
H	2.323513	5.019159	-0.317540
H	1.171180	6.036463	0.573659
H	1.045083	5.906857	-1.194152
C	1.813813	3.372906	-2.418392
H	0.898133	3.947013	-2.552769
H	1.888706	2.629251	-3.219311
H	2.679600	4.040087	-2.488459
C	2.800399	1.641636	-0.952919
H	2.779867	1.303031	0.081823
H	3.779289	2.077559	-1.182798
H	2.623461	0.786068	-1.613748
O	-0.510616	0.775325	-2.184867
H	-2.449289	2.080742	-1.442247
H	-2.771821	1.673971	0.264613
H	-4.122951	2.093551	-0.826313
H	-0.248738	0.553554	-3.103154

Table S17. DFT-optimized coordinates of $S = 2$ $\{FeCH_3NO\}^8$ complex

Fe	0.023233	-0.037641	0.215647
N	0.253760	0.126649	-1.767443
N	-0.028741	-0.076588	2.527299
N	-0.235796	2.002785	0.650992
N	1.883838	-0.913958	0.662103
N	-1.715617	-1.216559	0.569377
N	-0.834286	4.219237	0.004277
N	0.994517	3.165045	-0.975601
N	4.125253	-1.437844	0.046938
N	2.357656	-2.494653	-1.015799
N	-3.269705	-2.881714	-0.128514
N	-3.433030	-0.712205	-0.959314
C	-0.011516	1.336741	2.985209
H	1.028837	1.672693	3.007176
H	-0.418051	1.425346	4.002384
C	-0.795765	2.203635	2.006068
H	-1.859666	1.932579	2.042488
H	-0.718920	3.251843	2.313107
C	-0.043632	3.108798	-0.091997
C	-2.269879	4.149859	0.295885
H	-2.606062	3.117631	0.226481
H	-2.808743	4.751993	-0.443605
H	-2.496493	4.543657	1.292925
C	-0.298886	5.586066	-0.121906
H	0.789728	5.560393	-0.101821
H	-0.653133	6.173266	0.731386
H	-0.640637	6.069974	-1.043049
C	0.926508	3.911562	-2.238869
H	-0.107829	4.176459	-2.456749
H	1.309148	3.268687	-3.038493
H	1.537223	4.820694	-2.208063
C	2.302605	2.579870	-0.672246
H	2.279443	2.178715	0.340452
H	3.066642	3.363682	-0.739260
H	2.547503	1.782134	-1.379878
C	1.176717	-0.816547	2.986433
H	0.943245	-1.884528	2.980480
H	1.441415	-0.532089	4.014212
C	2.327399	-0.551856	2.026186
H	2.624384	0.504157	2.085186
H	3.195255	-1.148280	2.325393
C	2.773157	-1.582383	-0.097427
C	4.755765	-0.152041	0.361120

H	4.015248	0.642059	0.300984
H	5.543444	0.043416	-0.374529
H	5.208654	-0.161370	1.359015
C	5.062791	-2.561756	-0.112079
H	4.510879	-3.500704	-0.135425
H	5.739437	-2.568047	0.748687
H	5.662101	-2.464238	-1.023817
C	3.052836	-2.697170	-2.295743
H	3.840006	-1.954111	-2.408427
H	2.331275	-2.565495	-3.108325
H	3.479682	-3.703499	-2.360004
C	1.084641	-3.192748	-0.888293
C	-1.276388	-0.779180	2.924000
H	-2.093722	-0.052972	2.936454
H	-1.183104	-1.202519	3.933755
C	-1.583192	-1.863034	1.898573
H	-0.781684	-2.613556	1.901041
H	-2.509707	-2.374729	2.178261
C	-2.776968	-1.608651	-0.158473
C	-2.414386	-4.057759	0.064411
H	-1.371667	-3.768966	-0.042409
H	-2.661308	-4.799797	-0.702042
H	-2.572666	-4.511248	1.049237
C	-4.711851	-3.179524	-0.190885
H	-5.287061	-2.261610	-0.079293
H	-4.958127	-3.849663	0.638911
H	-4.981371	-3.674729	-1.129578
C	-4.122522	-1.107091	-2.195211
H	-3.773390	-2.088925	-2.514103
H	-3.885882	-0.373891	-2.973407
H	-5.210955	-1.129756	-2.071050
C	-3.704033	0.654623	-0.511305
H	-3.148808	0.842036	0.406268
H	-4.778769	0.780098	-0.327516
H	-3.407149	1.377141	-1.278647
O	1.380086	0.023404	-2.299019
H	0.325192	-2.767904	-1.556293
H	0.744611	-3.120559	0.144747
H	1.231152	-4.245378	-1.154109
C	-0.808664	0.500526	-2.743170
H	-1.297078	-0.421859	-3.073563
H	-1.541959	1.138335	-2.247834
H	-0.345095	0.996889	-3.597417

Table S18. DFT-optimized coordinates of $S = 1$ $\{FeCH_3NO\}^8$ complex

Fe	0.073475	-0.047539	0.309086
N	0.352814	-0.066190	-1.502186
N	-0.065972	-0.025758	2.420053
N	0.651544	1.902309	0.591387
N	1.267749	-1.643556	0.679046
N	-2.076005	-0.356884	0.512559
N	1.031484	4.142826	-0.112692
N	2.310578	2.414290	-0.998542
N	3.051907	-3.083092	0.044451
N	1.001006	-3.253680	-1.020227
N	-4.214051	-1.202044	-0.124181
N	-3.462859	0.816240	-0.994780
C	0.558447	1.245232	2.906033
H	1.641754	1.100815	2.930100
H	0.214408	1.467581	3.924384
C	0.218860	2.358542	1.931647
H	-0.858135	2.569931	1.958507
H	0.739076	3.276037	2.225531
C	1.307642	2.806148	-0.164947
C	-0.314917	4.669341	0.131658
H	-1.039338	3.862249	0.052650
H	-0.538809	5.427776	-0.626088
H	-0.389690	5.136894	1.119920
C	2.079706	5.171355	-0.234835
H	3.063073	4.706718	-0.179400
H	1.972505	5.872078	0.599394
H	1.987328	5.729940	-1.172243
C	2.587394	3.079519	-2.279175
H	1.764280	3.746246	-2.535685
H	2.681672	2.309875	-3.052438
H	3.521199	3.651624	-2.245864
C	3.277922	1.381418	-0.618534
H	3.017227	1.004225	0.369808
H	4.280966	1.824589	-0.590999
H	3.264930	0.561028	-1.339854
C	0.676173	-1.211335	2.965957
H	-0.012389	-2.059308	2.986080
H	1.003236	-1.006429	3.992998
C	1.833640	-1.526144	2.041568
H	2.590736	-0.732067	2.098406
H	2.316067	-2.458075	2.354102
C	1.772772	-2.624121	-0.096426
C	4.179705	-2.200526	0.358563

H	3.862085	-1.163360	0.281393
H	4.978487	-2.379079	-0.369232
H	4.575862	-2.395943	1.361597
C	3.405698	-4.502311	-0.124081
H	2.499718	-5.106782	-0.149713
H	4.014144	-4.808716	0.732975
H	3.985374	-4.669138	-1.038467
C	1.540365	-3.724156	-2.305061
H	2.571600	-3.393850	-2.414130
H	0.946737	-3.284709	-3.113164
H	1.488758	-4.815200	-2.381098
C	-0.448682	-3.326968	-0.894953
C	-1.499941	-0.102054	2.838144
H	-1.922656	0.905375	2.815202
H	-1.569747	-0.484291	3.864701
C	-2.238409	-0.981907	1.847619
H	-1.830649	-2.001486	1.873614
H	-3.293208	-1.046175	2.133411
C	-3.217342	-0.267294	-0.191011
C	-3.948681	-2.630875	0.067101
H	-2.886900	-2.822857	-0.065685
H	-4.511395	-3.196692	-0.682939
H	-4.262588	-2.968427	1.061502
C	-5.643199	-0.843898	-0.145282
H	-5.758007	0.234624	-0.046648
H	-6.131776	-1.328426	0.706340
H	-6.130513	-1.184813	-1.064894
C	-4.266965	0.734073	-2.222662
H	-4.399696	-0.309245	-2.506884
H	-3.733530	1.255779	-3.025230
H	-5.246918	1.208136	-2.100530
C	-3.067378	2.168600	-0.602397
H	-2.521940	2.113938	0.338412
H	-3.961005	2.793043	-0.480951
H	-2.432531	2.624722	-1.370269
O	1.371848	-0.544068	-2.044340
H	-0.945609	-2.611974	-1.561904
H	-0.724247	-3.112653	0.137146
H	-0.775002	-4.338039	-1.162414
C	-0.556558	0.590102	-2.488315
H	-0.547189	-0.004945	-3.403566
H	-1.552637	0.665328	-2.062078
H	-0.151440	1.583275	-2.703705

Table S19. DFT-optimized coordinates of $S = 2$ $\{FeNOCH_3\}^8$ complex

Fe	0.041851	-0.079202	0.352145
N	0.139775	0.047771	-1.394535
N	0.021032	-0.161011	2.543726
N	1.619012	-1.431309	0.679123
N	-1.892251	-0.697134	0.604954
N	0.427100	1.939575	0.784585
N	3.656462	-2.437404	-0.043959
N	1.673124	-2.863810	-1.175635
N	-3.876994	-1.763514	-0.151280
N	-3.303731	0.337905	-0.968245
N	0.446460	4.252248	0.199708
N	1.769110	2.744779	-0.967881
C	0.918404	-1.272665	2.983022
H	0.358492	-2.208286	2.909199
H	1.211993	-1.129078	4.031223
C	2.125814	-1.335216	2.062730
H	2.751435	-0.444032	2.206497
H	2.738874	-2.205198	2.322252
C	2.312184	-2.210852	-0.165495
C	4.598191	-1.411311	0.415064
H	4.106486	-0.440995	0.431867
H	5.438581	-1.367276	-0.285959
H	4.991772	-1.641811	1.411572
C	4.265432	-3.746288	-0.333183
H	3.485987	-4.498502	-0.449132
H	4.902284	-4.024796	0.512695
H	4.883907	-3.714661	-1.236891
C	2.303678	-3.121560	-2.475281
H	3.240959	-2.570995	-2.546750
H	1.629601	-2.776407	-3.266331
H	2.494676	-4.189565	-2.627634
C	0.287827	-3.308581	-1.050726
H	-0.002482	-3.263582	-0.001171
H	0.215322	-4.342363	-1.407159
H	-0.386182	-2.677598	-1.639337
C	-1.386475	-0.431564	2.958597
H	-1.925907	0.518711	2.983130
H	-1.412158	-0.868555	3.965719
C	-2.026735	-1.350737	1.931093
H	-1.537712	-2.333409	1.945267
H	-3.080139	-1.507065	2.184100
C	-2.996423	-0.718246	-0.169430
C	-3.439525	-3.151864	0.030260

H	-2.357902	-3.208545	-0.075413
H	-3.906584	-3.771505	-0.742414
H	-3.735228	-3.541978	1.010771
C	-5.337228	-1.576877	-0.211121
H	-5.580614	-0.521229	-0.097390
H	-5.788928	-2.132522	0.617041
H	-5.755914	-1.953439	-1.150361
C	-4.086793	0.206802	-2.203980
H	-4.131290	-0.838863	-2.506863
H	-3.594107	0.788774	-2.988497
H	-5.104238	0.593534	-2.081003
C	-2.930535	1.709047	-0.617639
C	0.505927	1.148870	3.072062
H	1.598512	1.128012	3.068608
H	0.168124	1.290563	4.107313
C	0.020667	2.269124	2.166097
H	-1.069977	2.371054	2.252864
H	0.458962	3.217971	2.493877
C	0.853821	2.956950	0.016442
C	-0.915369	4.615201	0.602293
H	-1.558037	3.738958	0.561478
H	-1.300969	5.367579	-0.094504
H	-0.936455	5.039053	1.612772
C	1.356283	5.395383	0.019156
H	2.382057	5.039980	-0.070304
H	1.279778	6.039546	0.901279
H	1.093876	5.986545	-0.865159
C	1.760165	3.496212	-2.228675
H	0.855827	4.099876	-2.292775
H	1.766781	2.781269	-3.058082
H	2.639794	4.143397	-2.318042
C	2.799126	1.713837	-0.867086
H	2.782989	1.302232	0.140983
H	3.776485	2.169230	-1.067671
H	2.623096	0.908284	-1.586749
O	-0.430031	0.682323	-2.420861
H	-2.192415	2.101606	-1.322559
H	-2.511384	1.710117	0.387335
H	-3.827312	2.338693	-0.647550
C	-0.748805	-0.201130	-3.553600
H	-1.213513	0.446902	-4.296704
H	-1.431825	-0.986264	-3.224557
H	0.180572	-0.623741	-3.939219

Table S20. DFT-optimized coordinates for $S = 1$ $\{FeNOCH_3\}^8$ complex

Fe	0.011011	-0.045771	0.395716
N	0.171919	-0.127224	-1.334033
N	0.034340	-0.124409	2.547511
N	1.563339	-1.406465	0.663887
N	-1.920886	-0.702276	0.699203
N	0.388579	1.919125	0.729537
N	3.558982	-2.477165	-0.091306
N	1.548116	-2.863192	-1.178885
N	-3.856353	-1.873040	-0.042981
N	-3.336879	0.207539	-0.940189
N	0.425968	4.212058	0.099207
N	1.811097	2.694776	-0.980920
C	0.950888	-1.219730	2.991049
H	0.391897	-2.158377	2.961209
H	1.279726	-1.046742	4.024081
C	2.121694	-1.299905	2.028407
H	2.754902	-0.408671	2.138128
H	2.742214	-2.168256	2.274747
C	2.218094	-2.211575	-0.189722
C	4.546663	-1.478018	0.326749
H	4.084587	-0.494201	0.363800
H	5.359764	-1.457269	-0.407173
H	4.973407	-1.720074	1.306771
C	4.120182	-3.806812	-0.382917
H	3.314946	-4.534830	-0.474597
H	4.768455	-4.097838	0.450161
H	4.717778	-3.802359	-1.301235
C	2.139423	-3.120454	-2.496783
H	3.103496	-2.619603	-2.574148
H	1.468947	-2.718828	-3.264411
H	2.270004	-4.193317	-2.675318
C	0.150153	-3.253492	-1.038502
H	-0.130784	-3.171502	0.011035
H	0.038808	-4.292108	-1.370608
H	-0.502193	-2.611525	-1.640153
C	-1.357760	-0.390549	3.021921
H	-1.899417	0.558223	3.044800
H	-1.340396	-0.804160	4.038576
C	-2.027435	-1.330544	2.036301
H	-1.538628	-2.313544	2.062858
H	-3.075166	-1.479789	2.317013
C	-3.006662	-0.802876	-0.088907
C	-3.398832	-3.242500	0.212474

H	-2.314312	-3.284205	0.143818
H	-3.828785	-3.904149	-0.547006
H	-3.719913	-3.595270	1.199164
C	-5.316217	-1.728509	-0.176694
H	-5.590735	-0.675856	-0.121513
H	-5.792036	-2.260676	0.653376
H	-5.680101	-2.156069	-1.117111
C	-4.017091	-0.023540	-2.219562
H	-3.980389	-1.083147	-2.471320
H	-3.498054	0.546721	-2.996699
H	-5.060931	0.308712	-2.192144
C	-3.121603	1.612677	-0.592723
C	0.514029	1.204200	3.036498
H	1.606665	1.202392	3.007087
H	0.196897	1.366174	4.075045
C	-0.014698	2.284288	2.107644
H	-1.106293	2.358178	2.197333
H	0.403178	3.253932	2.396799
C	0.852272	2.920353	-0.043631
C	-0.954373	4.559934	0.451488
H	-1.582779	3.674749	0.385082
H	-1.320297	5.308991	-0.258954
H	-1.017017	4.982450	1.460752
C	1.335283	5.362747	-0.037014
H	2.367453	5.016318	-0.072384
H	1.209073	6.006784	0.839395
H	1.112546	5.950559	-0.934045
C	1.885292	3.455224	-2.234922
H	0.974164	4.036958	-2.368688
H	1.982516	2.748812	-3.065677
H	2.752576	4.124112	-2.250997
C	2.819413	1.649050	-0.826064
H	2.783822	1.278214	0.197189
H	3.806547	2.078217	-1.032621
H	2.638294	0.816069	-1.513863
O	-0.486665	0.764278	-2.108507
H	-2.412847	2.078580	-1.281683
H	-2.731679	1.664645	0.422940
H	-4.079349	2.144316	-0.647367
C	-0.280462	0.492759	-3.538381
H	-0.667850	1.369374	-4.058009
H	-0.841553	-0.402272	-3.814461
H	0.784521	0.355571	-3.729819

Table S21. DFT-optimized coordinates for the 4-coordinate $S = 1$ H{FeNO}^{8} complex

Fe	0.45891407518209	0.43784799231525	0.98046076238232
N	1.42559308581299	0.00555199435606	-0.29876656922562
O	1.91852190735365	-0.46402233922672	-1.29348853140722
N	0.24387997237419	0.40385201086669	3.13417913810023
N	3.80517243147396	-0.48953948874563	4.12689505439014
N	-0.94401513779137	-1.01924695283020	1.07262261209727
N	-0.02026156318079	2.39613108296677	1.19171758744312
N	4.86572696276847	-1.73150462482421	2.44465055699551
N	6.10488800511448	-0.83967718753324	4.21933625806075
N	-1.67424383171220	-3.06775196447824	0.11364201333202
N	-1.86403496740770	-1.07435876624939	-1.07685815023648
N	-0.91461500755199	4.39252221150448	0.27639889129165
N	1.11808171781656	3.56043387277068	-0.49433264522164
C	1.36350441085627	-0.24182274168175	3.88460585814312
H	1.25557554123934	-1.32430241829989	3.78038970113095
H	1.27398905355464	0.00074367406865	4.95284852835961
C	2.73897609484024	0.17778684806102	3.35851788773959
H	2.83902375520257	-0.09104342633678	2.30554410686620
H	2.88085483571124	1.26035798278358	3.44136492465925
C	4.93014032473464	-1.01648644116699	3.58798248700211
C	5.96189854614130	-1.74027251173389	1.46453147643672
H	5.54006677590314	-1.50642612930580	0.48200541963659
H	6.44120104371556	-2.72314689903279	1.42064147883153
H	6.69536151085681	-0.97948940967591	1.72795739486799
C	3.68510455894880	-2.52763285975910	2.08516812514706
H	3.14406709318549	-2.07518261989975	1.24672726444102
H	3.03036011055390	-2.61775911109830	2.95139690480476
H	4.02397643810466	-3.52427616919121	1.78690617652807
C	7.16029543038977	-1.86570995572246	4.21334777663104
H	7.43022387221839	-2.07816590172121	5.25209718902632
H	8.04484244149263	-1.50729892694681	3.67894999786629
H	6.78601273601712	-2.77612792776909	3.74809016020273
C	6.33074325710278	0.29002977165209	5.13445422457080
H	5.66300132262931	1.11341492366159	4.88045251962892
H	7.36564680174487	0.61895130751005	5.01264959933654
H	6.17389545130408	-0.01405469058917	6.17537870828595
C	-1.02573265899953	-0.35734477206730	3.39036494276488
H	-1.86168417342799	0.31783761471405	3.19517500163257
H	-1.07071360213939	-0.67447346883538	4.44012966853927
C	-1.10642869042664	-1.54531770972245	2.44358542367986
C	-1.46827968931975	-1.71297012882580	0.06175159797234
C	-0.71000282240358	-3.96893556791712	0.74808095764925
H	0.22883079708956	-3.44013115708698	0.91434983722160

H	-0.52137228904182	-4.80833071511556	0.06977874812252
H	-1.08367483458053	-4.36532378308957	1.69980976606732
C	-2.83493023897182	-3.71476649365040	-0.50664894627710
H	-3.55153059987765	-2.95481051953177	-0.81795622836134
H	-3.30685039995610	-4.37036773604567	0.23376998238786
H	-2.54406134171952	-4.32001044675733	-1.37380474937144
C	-1.68338774369429	-1.67041348447908	-2.40546065235064
H	-1.21369323056843	-2.64861581060323	-2.31111496262567
H	-1.03112114831897	-1.02108691442241	-3.00117119722858
H	-2.64421039016471	-1.77388366155383	-2.92147417341440
C	-2.19200291828755	0.34903742131622	-1.07214539633717
C	0.07829565685372	1.83557902064619	3.55085788145854
H	1.07361536884754	2.27283627598776	3.65302640378139
H	-0.42832345048769	1.88577098172684	4.52374326168210
C	-0.70034258479083	2.60455728401358	2.48658363861074
H	-1.74026069333602	2.25539950264528	2.45741087665277
H	-0.71883191935770	3.66649646077069	2.75636803036085
C	0.04996990740631	3.42439171256826	0.34225352024902
C	-2.33234853955136	4.09034915304945	0.48629808119752
H	-2.48100635464559	3.01164169715409	0.47580152151870
H	-2.90884711999121	4.53545858496034	-0.33211565844052
H	-2.69582713786237	4.50092612869087	1.43550026391221
C	-0.60565746420666	5.80019617891028	0.00139984387249
H	0.47248374293018	5.95242859181548	0.04209252476359
H	-1.08231428008567	6.41693420537459	0.77132469601826
H	-0.98389032180676	6.11008092579558	-0.97975967320305
C	0.98592121272997	4.08845704316604	-1.85530510012552
H	-0.06774689800759	4.22196356717290	-2.09854783608446
H	1.42427945628651	3.36743262100492	-2.55473996456664
H	1.51066134793930	5.04462220473615	-1.96574158695593
C	2.46178134947420	3.11204164553547	-0.12792995850851
H	2.47175525538935	2.82745500852539	0.92322061494316
H	3.16244122491885	3.93911705615081	-0.29545569431778
H	2.77382848867845	2.25751005004930	-0.73618175797008
H	-1.32459950187521	0.96181501033368	-1.34748672411507
H	-2.52772321419229	0.63454336331105	-0.07560681394201
H	-2.99588273562403	0.51840729067727	-1.79642875718015
H	3.87324133185195	-0.22310005815888	5.10311407854053
H	-0.33047479022349	-2.27744041614293	2.70217195141487
H	-2.07468041915300	-2.04616796549521	2.55864782821658

Table S22. DFT-optimized coordinates for the 5-coordinate $S = 1$ H{FeNO}^{8} CH_3CN-bound complex

Fe	1.04351030201559	0.04090186579194	0.08964386414852
N	1.82931095755244	-0.30264161189418	1.55050427270581
O	2.03226350145419	-1.02998537686623	2.49008885040671
N	-0.21767797365098	0.62270268912381	-2.02981251709381
N	-3.92046571153500	0.59041598586891	-2.91471026085808
N	1.65247761462971	-1.42255402118519	-1.24217985072619
N	1.42602185156794	2.07046400995413	-0.26137551813617
N	-4.58135763324070	-0.47941608777098	-4.88912586964714
N	-5.75369126666180	-0.84100143651798	-2.89231281458629
N	2.46298964066911	-3.64823705807167	-1.37818377696400
N	3.82523235222540	-1.95483694752582	-0.53745658761323
N	2.87421529442358	3.86397044536696	0.33304508797133
N	1.36830742903974	2.99249032255034	1.88364256027904
C	-1.67426101003424	0.39025150867699	-1.93384130169014
H	-2.04380122409063	0.96539320488922	-1.07848852579432
H	-1.84116700426520	-0.66857297556048	-1.72125125718853
C	-2.48809563894762	0.77886535399995	-3.18829003130393
H	-2.30817497143367	1.82156016582595	-3.46576892520327
H	-2.22792045422122	0.14391634944398	-4.03476506536544
C	-4.75223053623058	-0.24486436797806	-3.57054737941514
C	-4.89226528031671	-1.77983810701098	-5.49905843357768
H	-4.02646008212142	-2.09129918719325	-6.09161213093364
H	-5.76511797708864	-1.70915557742521	-6.15592242822602
H	-5.07431262726775	-2.51627651521474	-4.71714986240902
C	-4.08818002455705	0.55651716502337	-5.80864793059492
H	-3.09854415835479	0.29552428943728	-6.19702727419255
H	-4.04514817029469	1.51508001326478	-5.29287862386312
H	-4.78887056737908	0.63126745443025	-6.64610860002556
C	-7.06062242053376	-1.11247952810406	-3.51217451208735
H	-7.83403057800621	-0.64039282939242	-2.89854701137941
H	-7.24881090371344	-2.18900220171064	-3.56096123686050
H	-7.08967741242658	-0.68306322083775	-4.51231016070832
C	-5.69776264748530	-1.02176144777399	-1.43480798125501
H	-4.65803340730988	-1.08927410791871	-1.11371801983220
H	-6.20973529601443	-1.95568100065967	-1.19087791164118
H	-6.19602842495184	-0.19604978479519	-0.91415794106565
C	0.43384410232991	-0.29214562367378	-3.00250070902570
H	1.38391548282253	0.15826427054603	-3.30262109093802
H	-0.17402535967695	-0.42314180387757	-3.90901172341396
C	0.71233424196845	-1.64340203744538	-2.35023484211408
C	2.61189744367899	-2.32024171677996	-1.05413592440708
C	1.18753600577111	-4.33985595690027	-1.19070225994050
H	0.52490268002451	-3.71955236129379	-0.58697321111649

H	1.37239870582309	-5.28136352345222	-0.66035456302697
H	0.70136087014541	-4.56869794083882	-2.14736732486882
C	3.55380635621364	-4.46012584290357	-1.92274813609085
H	4.40717789613177	-3.82003449465044	-2.14645624931301
H	3.21350680850072	-4.93809616968608	-2.84914420067699
H	3.86151725207490	-5.24403467770058	-1.21954923461151
C	4.56431658698428	-2.80397672577956	0.40019200908163
H	3.99625666110986	-3.71192478293897	0.60037520523624
H	4.70713712347285	-2.26118915613013	1.34232015797145
H	5.54810648503165	-3.07173801132254	-0.00283004712731
C	4.34425821601232	-0.59948678766177	-0.69748081199055
C	0.09528710196579	2.05141274807201	-2.28665923242395
H	-0.67882034940323	2.65118912243317	-1.79798721712436
H	0.08310283081127	2.28352595543704	-3.36184470263544
C	1.45043939138683	2.41977221538848	-1.68782698289693
H	2.24750276741401	1.87777908800678	-2.21559408848423
H	1.62714657367979	3.49128505432615	-1.83999542457906
C	1.88892623246713	2.94831328480707	0.61872976898886
C	3.99001874867231	3.53972351787463	-0.55538435683697
H	3.97655854442743	2.47404702357818	-0.78014539628180
H	4.93113205092292	3.78217106135609	-0.04747234053432
H	3.94162800747167	4.10914057996142	-1.49152270822819
C	2.89134359411869	5.21316492675324	0.90321442739371
H	1.95065035002427	5.40205367231289	1.42032929021106
H	3.00428272984463	5.93943835568793	0.08970687932836
H	3.72469073226698	5.34506941842217	1.60466624251185
C	2.20569929466768	3.22059494012642	3.06425716738287
H	3.24551622181026	3.34113724767533	2.76196174703024
H	2.13027423715727	2.35276881066427	3.73082510305899
H	1.88015585765252	4.11204219416166	3.61296762423730
C	0.00633682650456	2.54191418338690	2.16426939752357
H	-0.57118906287917	2.54665002404933	1.24027263118235
H	-0.44398909030205	3.23209138764348	2.88730594350288
H	-0.00503423781532	1.52944350459096	2.58463176496632
H	4.21043743759307	-0.00638939004515	0.21480950936949
H	3.81952564799784	-0.11384676178676	-1.52036175673391
H	5.41459297572267	-0.65979124836836	-0.92728580210258
H	-4.28092446712530	1.02186565026203	-2.07057043919738
N	-0.62272000359531	-0.84548989211114	0.66855734569551
C	-1.51235914065649	-1.39673761957710	1.17486997137901
C	-2.63062848396833	-2.07396273525764	1.81246350363990
H	-2.29480734052199	-2.51526553371024	2.75576929562564
H	-3.01112773440849	-2.86831926571930	1.16294284516157
H	-3.43166393466322	-1.35774040373106	2.02069803392812
H	-0.23109290129281	-2.08181062703931	-1.99785005007721

H	1.13607549218851	-2.32603457938288	-3.09707993288239

Table S23. DFT-optimized coordinates of $[Fe(TMG_3tren)(CN)]^{3+}$ (S = 1)

Fe	0.013523	4.151437	3.289827
N	-1.012770	5.902901	3.156437
N	1.294018	5.167571	4.153940
N	-0.056516	4.170354	1.441887
N	-1.458824	3.561446	4.240769
N	3.621687	5.659070	4.047478
N	2.917158	3.805544	5.262431
N	1.441102	2.577383	0.472975
N	-0.710933	2.786400	-0.382463
N	-2.012558	2.534251	6.316663
N	-1.459438	1.184508	4.505989
N	1.565445	1.501720	3.489472
C	-0.542998	6.765760	4.281930
H	-1.024017	6.410295	5.195829
H	-0.833232	7.811223	4.126191
C	0.962267	6.610438	4.380242
H	1.467931	7.247923	3.648106
H	1.315590	6.915770	5.371037
C	2.631432	4.845840	4.476231
C	3.587849	6.390631	2.770587
H	2.690914	6.128461	2.211810
H	4.471354	6.116166	2.185468
H	3.619079	7.469549	2.952753
C	4.847266	5.907261	4.846045
H	4.697273	5.567685	5.869369
H	5.022236	6.986683	4.845509
H	5.716358	5.409978	4.406620
C	4.182924	3.046153	5.162063
H	4.728142	3.345654	4.269476
H	3.909188	1.990432	5.079828
H	4.801792	3.193846	6.050934
C	1.999622	3.296607	6.290616
H	1.116083	3.927934	6.332236
H	2.517003	3.325401	7.255028
H	1.726199	2.266490	6.052217
C	-0.687160	6.494682	1.823828
H	0.307639	6.940217	1.892278
H	-1.398905	7.284726	1.557858
C	-0.695072	5.368205	0.808703
H	-1.716240	5.142509	0.485590
H	-0.130514	5.653529	-0.085515
C	0.231492	3.140016	0.519046
C	2.670853	3.276671	0.868829
H	2.434391	4.303840	1.133356
H	3.359010	3.266338	0.017394
H	3.126025	2.755948	1.713998
C	1.661566	1.181457	0.035237
H	0.708676	0.664802	-0.058113
H	2.258175	0.699166	0.814719

H	2.204913	1.147542	-0.912698
C	-2.157144	2.807847	-0.109447
H	-2.338904	3.084782	0.927756
H	-2.563819	1.808267	-0.293137
H	-2.658087	3.510632	-0.782783
C	-0.369163	2.353377	-1.759797
H	0.663921	2.613340	-1.983742
H	-1.033120	2.890063	-2.443088
H	-0.524942	1.278882	-1.889791
C	-2.462738	5.564305	3.278426
H	-2.789828	5.155538	2.319948
H	-3.060568	6.457858	3.492113
C	-2.599203	4.523589	4.372762
H	-2.601061	4.995275	5.360463
H	-3.546737	3.983357	4.272491
C	-1.615109	2.401506	5.032038
C	-1.639267	3.667368	7.178897
H	-0.956114	4.331136	6.651356
H	-1.145337	3.278440	8.075018
H	-2.534198	4.214920	7.491238
C	-2.891655	1.541430	6.982155
H	-3.344837	0.890169	6.236870
H	-3.676804	2.098796	7.500455
H	-2.338722	0.948327	7.715770
C	-1.005004	0.019563	5.296719
H	-0.661327	0.344593	6.276489
H	-0.167749	-0.423055	4.749681
H	-1.803048	-0.720054	5.401812
C	-1.705119	0.881124	3.089841
H	-2.072507	1.771803	2.587097
H	-2.460915	0.090894	3.035519
H	-0.777928	0.533492	2.629198
C	0.975037	2.509965	3.413835

Table S24. DFT-optimized coordinates for $[Fe(TMG_3tren)(CH_3CN)]^{2+}$ ($S = 2$)

Fe	11.697098	0.066812	3.578263
N	10.405154	-0.007929	5.435987
N	13.185217	0.253210	5.076572
N	15.363956	0.852209	5.843988
N	15.097615	-0.808505	4.236781
N	10.517789	1.806988	3.280429
N	9.544521	3.482040	1.884597
N	11.847614	3.399282	2.188741
N	10.770133	-1.801924	3.286146
N	10.459781	-2.088734	0.980541
N	10.687355	-3.978212	2.319086
N	12.885220	0.141440	1.850023
C	11.319305	-0.128413	6.600922
H	11.592236	-1.181707	6.709777
H	10.820943	0.190379	7.527569
C	12.582354	0.691113	6.353842
H	12.329329	1.759970	6.329216
H	13.274407	0.543081	7.189795
C	14.514526	0.120549	5.055499
C	15.107609	2.253176	6.191452
H	14.295806	2.639996	5.578313
H	16.012276	2.837372	5.990153
H	14.852009	2.368154	7.251009
C	16.569511	0.273413	6.458305
H	16.572611	-0.807099	6.319192
H	16.551281	0.489287	7.531809
H	17.485069	0.701486	6.034926
C	14.447002	-2.077856	3.922800
H	13.552655	-2.174400	4.537294
H	15.137897	-2.900758	4.143111
H	14.164170	-2.132388	2.865496
C	16.412145	-0.607416	3.621735
H	16.732427	0.424409	3.763094
H	16.334702	-0.812473	2.547315
H	17.166962	-1.282103	4.041609
C	9.618703	1.253548	5.481291
H	10.236855	2.021373	5.954459
H	8.711617	1.128843	6.089523
C	9.268571	1.697961	4.065085
H	8.577109	0.973225	3.613247
H	8.742908	2.658069	4.112766
C	10.620339	2.860397	2.465045
C	9.470513	4.941891	1.714490
H	10.294563	5.417593	2.245100
H	8.526378	5.295376	2.142447
H	9.499741	5.228674	0.657248
C	8.354409	2.749025	1.443899
H	8.559456	1.680086	1.452267
H	8.111682	3.054411	0.420127

H	7.487459	2.959601	2.080675
C	12.936904	3.370323	3.159810
H	12.538087	3.057534	4.123897
H	13.367135	4.375120	3.245911
H	13.729524	2.675742	2.857285
C	12.173531	4.004893	0.894859
H	11.374324	3.805620	0.181640
H	13.104148	3.561997	0.520024
H	12.323222	5.087361	0.978196
C	9.528680	-1.200216	5.297177
H	8.661523	-0.914924	4.695270
H	9.164504	-1.536319	6.278430
C	10.284170	-2.317949	4.585008
H	11.116663	-2.661733	5.213650
H	9.612522	-3.171148	4.441660
C	10.651651	-2.611977	2.229068
C	9.734645	-0.837804	0.771844
H	9.260526	-0.547083	1.708548
H	8.968929	-0.991447	0.002428
H	10.404999	-0.035070	0.443918
C	10.985100	-2.721825	-0.232623
H	11.667820	-3.527098	0.036653
H	11.531508	-1.970614	-0.815157
H	10.182708	-3.121633	-0.862804
C	9.827515	-4.848671	1.500990
H	9.094213	-4.246000	0.966323
H	9.297578	-5.538961	2.165753
H	10.412326	-5.437285	0.785414
C	11.537460	-4.679765	3.285992
H	12.250919	-3.980873	3.719338
H	12.087935	-5.468729	2.762185
H	10.947734	-5.143244	4.085110
C	13.535423	0.198645	0.890739
C	14.352227	0.275276	-0.313451
H	13.769541	0.691119	-1.141285
H	14.706107	-0.722652	-0.590416
H	15.218666	0.918549	-0.130661

References

(1) Saba, S.; Hernandez, R.; Choy, C. C.; Carta, K.; Bennett, Y.; Bondi, S.; Kolaj, S.; Bennett, C. A simple and efficient one-step protocol for the preparation of alkyl-substituted ammonium tetrafluoroborate and hexafluorophosphate salts *J. Fluorine Chem.* **2013**, *153*, 168-171.

(2) Speelman, A. L.; Lehnert, N. Characterization of a High-Spin Non-Heme $\{FeNO\}^8$ Complex: Implications for the Reactivity of Iron Nitroxyl Species in Biology *Angew. Chem. Int. Ed.* **2013**, *52*, 12283-12287.

(3) Speelman, A. L.; Zhang, B.; Krebs, C.; Lehnert, N. Structural and Spectroscopic Characterization of a High-Spin $\{FeNO\}^6$ Complex with an Iron(IV)−NO^- Electronic Structure *Angew. Chem. Int. Ed.* **2016**, *55*, 6685-6688.

(4) England, J.; Guo, Y.; Van Heuvelen, K. M.; Cranswick, M. A.; Rohde, G. T.; Bominaar, E. L.; Münck, E.; Que, L. A More Reactive Trigonal-Bipyramidal High-Spin Oxoiron(IV) Complex with a cis-Labile Site *J. Am. Chem. Soc.* **2011**, *133*, 11880-11883.

(5) Sage, J. T.; Paxson, C.; Wyllie, G. R. A.; Sturhahn, W.; Durbin, S. M.; Champion, P. M.; Alp, E. E.; Scheidt, W. R. Nuclear resonance vibrational spectroscopy of a protein active-site mimic *J. Phys.: Condens. Matter* **2001**, *13*, 7707.

(6) Sturhahn, W. Nuclear resonant spectroscopy *J. Phys. Condens. Matter* **2004**, *16*, S497-S530.

(7) Paulat, F.; Lehnert, N. Detailed Assignment of the Magnetic Circular Dichroism and UV−vis Spectra of Five-Coordinate High-Spin Ferric [Fe(TPP)(Cl)] *Inorg. Chem.* **2008**, *47*, 4963-4976.

(8) Galinato, M. G. I.; Spolitak, T.; Ballou, D. P.; Lehnert, N. Elucidating the Role of the Proximal Cysteine Hydrogen-Bonding Network in Ferric Cytochrome P450cam and Corresponding Mutants Using Magnetic Circular Dichroism Spectroscopy *Biochemistry* **2011**, *50*, 1053-1069.

(9) Neese, F.; Solomon, E. I. MCD C-Term Signs, Saturation Behavior, and Determination of Band Polarizations in Randomly Oriented Systems with Spin $S \geq 1/2$. Applications to $S = 1/2$ and $S = 5/2$ *Inorg. Chem.* **1999**, *38*, 1847-1865.

(10) George, G. N. G., S. J.; Pickering, I. J. *EXAFSPAK* http://ssrl.slac.stanford.edu/exafspak.html, 2001.

(11) Weng, T.-C.; Waldo, G. S.; Penner-Hahn, J. E. A method for normalization of X-ray absorption spectra *Journal of Synchrotron Radiation* **2005**, *12*, 506-510.

(12) Rehr, J. J.; Kas, J. J.; Vila, F. D.; Prange, M. P.; Jorissen, K. Parameter-free calculations of X-ray spectra with FEFF9 *PCCP* **2010**, *12*, 5503-5513.

(13) Bhave, D. P.; Han, W.-G.; Pazicni, S.; Penner-Hahn, J. E.; Carroll, K. S.; Noodleman, L. Geometric and Electrostatic Study of the [4Fe-4S] Cluster of Adenosine-5′-Phosphosulfate Reductase from Broken Symmetry Density Functional Calculations and Extended X-ray Absorption Fine Structure Spectroscopy *Inorg. Chem.* **2011**, *50*, 6610-6625.

(14) Neese, F. The ORCA program system *Wiley Interdiscip. Rev.: Comput. Mol. Sci.* **2012**, *2*, 73-78.

(15) Römelt, M.; Ye, S.; Neese, F. Calibration of Modern Density Functional Theory Methods for the Prediction of 57Fe Mössbauer Isomer Shifts: Meta-GGA and Double-Hybrid Functionals *Inorg. Chem.* **2009**, *48*, 784-785.

(16) Frisch, M. J.; Trucks, G. W.; Schlegel, H. B.; Scuseria, G. E.; Robb, M. A.; Cheeseman, J. R.; Scalmani, G.; Barone, V.; Mennucci, B.; Petersson, G. A.; Nakatsuji, H.; Caricato, M.; Li, X.; Hratchian, H. P.; Izmaylov, A. F.; Bloino, J.; Zheng, G.; Sonnenberg, J. L.; Hada, M.; Ehara, M.; Toyota, K.; Fukuda, R.; Hasegawa, J.; Ishida, M.; Nakajima, T.; Honda, Y.; Kitao, O.; Nakai, H.; Vreven, T.; Montgomery, J. A.; Peralta, J. E.; Ogliaro, F.; Bearpark, M.; Heyd, J. J.; Brothers, E.; Kudin, K. N.; Staroverov, V. N.; Kobayashi, R.; Normand, J.; Raghavachari, K.; Rendell, A.; Burant, J. C.; Iyengar, S. S.; Tomasi, J.; Cossi, M.; Rega, N.; Millam, J. M.; Klene, M.; Knox, J. E.; Cross, J. B.; Bakken, V.; Adamo, C.; Jaramillo, J.; Gomperts, R.; Stratmann, R. E.; Yazyev, O.; Austin, A. J.; Cammi, R.; Pomelli, C.; Ochterski, J. W.; Martin, R. L.; Morokuma, K.; Zakrzewski, V. G.; Voth, G. A.; Salvador, P.; Dannenberg, J. J.; Dapprich, S.; Daniels, A. D.; Farkas; Foresman, J. B.; Ortiz, J. V.; Cioslowski, J.; Fox, D. J. *Gaussian 09, Revision B.01*, Wallingford CT, 2009.

(17) Allouche, A.; Pourcin, J. Ab initio calculation of vibrational force fields: Determination of non-redundant symmetry coordinates by least-square component analysis *Spectrochim. Acta A* **1993**, *49*, 571-580.

(18) Paulat, F.; Berto, T. C.; DeBeer George, S.; Goodrich, L.; Praneeth, V. K. K.; Sulok, C. D.; Lehnert, N. Vibrational Assignments of Six-Coordinate Ferrous Heme Nitrosyls: New Insight from Nuclear Resonance Vibrational Spectroscopy *Inorg. Chem.* **2008**, *47*, 11449-11451.

(19) McIntosh, D. F.; Peterson, M. R. *QCPE 576* University of Indiana, Bloomington, Indiana.

(20) Lehnert, N. In *Computational Inorganic and Bioinorganic Chemistry*; Solomon, E. I., King, R. B., Scott, R. A., Eds.; John Wiley & Sons: Chichester, UK, 2009, p 123-140.

(21) Wittmann, H.; Raab, V.; Schorm, A.; Plackmeyer, J.; Sundermeyer, J. Complexes of Manganese, Iron, Zinc, and Molybdenum with a Superbasic Tris(guanidine) Derivative of Tris(2-ethylamino)amine (Tren) as a Tripod Ligand *Eur. J. Inorg. Chem.* **2001**, *2001*, 1937-1948.
(22) England, J.; Guo, Y.; Farquhar, E. R.; Young Jr, V. G.; Münck, E.; Que Jr, L. The Crystal Structure of a High-Spin Oxoiron(IV) Complex and Characterization of Its Self-Decay Pathway *J. Am. Chem. Soc.* **2010**, *132*, 8635-8644.
(23) Choi, I. K.; Liu, Y.; Feng, D.; Paeng, K. J.; Ryan, M. D. Electrochemical and spectroscopic studies of iron porphyrin nitrosyls and their reduction products *Inorg. Chem.* **1991**, *30*, 1832-1839.
(24) Pellegrino, J.; Bari, S. E.; Bikiel, D. E.; Doctorovich, F. Successful Stabilization of the Elusive Species $\{FeNO\}^8$ in a Heme Model *J. Am. Chem. Soc.* **2009**, *132*, 989-995.
(25) Goodrich, L. E.; Roy, S.; Alp, E. E.; Zhao, J.; Hu, M. Y.; Lehnert, N. Electronic Structure and Biologically Relevant Reactivity of Low-Spin {FeNO}8 Porphyrin Model Complexes: New Insight from a Bis-Picket Fence Porphyrin *Inorg. Chem.* **2013**, *52*, 7766-7780.
(26) Abucayon, E. G.; Khade, R. L.; Powell, D. R.; Zhang, Y.; Richter-Addo, G. B. Hydride Attack on a Coordinated Ferric Nitrosyl: Experimental and DFT Evidence for the Formation of a Heme Model–HNO Derivative *J. Am. Chem. Soc.* **2016**, *138*, 104-107.
(27) England, J.; Martinho, M.; Farquhar, E. R.; Frisch, J. R.; Bominaar, E. L.; Münck, E.; Que, L. A Synthetic High-Spin Oxoiron(IV) Complex: Generation, Spectroscopic Characterization, and Reactivity *Angew. Chem. Int. Ed.* **2009**, *48*, 3622-3626.
(28) England, J.; Farquhar, E. R.; Guo, Y.; Cranswick, M. A.; Ray, K.; Münck, E.; Que, L. Characterization of a Tricationic Trigonal Bipyramidal Iron(IV) Cyanide Complex, with a Very High Reduction Potential, and Its Iron(II) and Iron(III) Congeners *Inorg. Chem.* **2011**, *50*, 2885-2896.